AD-A192 827 ANALYSIS OF EXPERIMENTAL DATA FOR CAST 10-2/DOA2 SUPERCRITICAL AIRFOIL AT.. (U) NATIONAL AERONAUTICAL ESTABLISHMENT OTTAWA (ONTARIO) Y Y CHAN JAN 88 1/1

UNCLASSIFIED NAE-AN-49 NRC-28595 F/G 20/4 NL

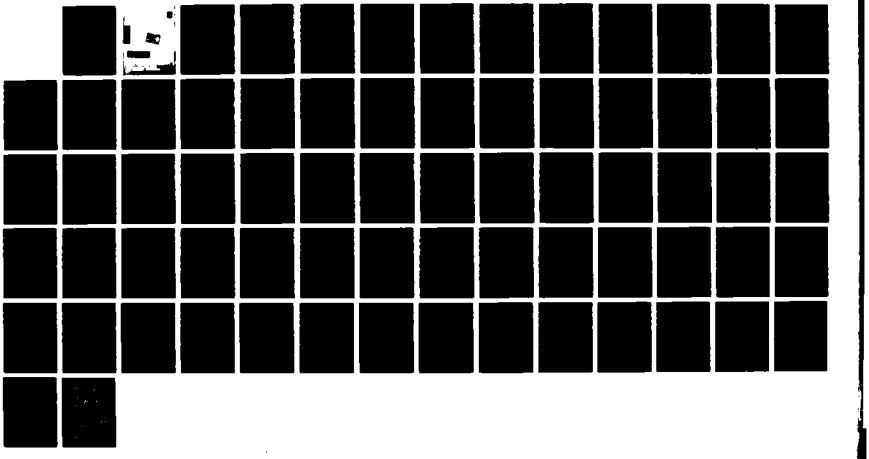

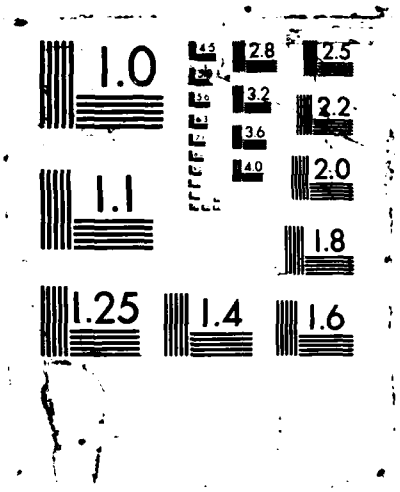
1.0
1.1
1.25
1.4
1.6
1.8
2.0
2.2
2.5
2.8
3.2
3.6
4.0


DTIC
ELECTE
MAR 2 4 1988
S
D
D

NATIONAL AERONAUTICAL ESTABLISHMENT

SCIENTIFIC AND TECHNICAL PUBLICATIONS

AERONAUTICAL REPORTS:

Aeronautical Reports (LR): Scientific and technical information pertaining to aeronautics considered important, complete, and a lasting contribution to existing knowledge.

Mechanical Engineering Reports (MS): Scientific and technical information pertaining to investigations outside aeronautics considered important, complete, and a lasting contribution to existing knowledge.

AERONAUTICAL NOTES (AN): Information less broad in scope but nevertheless of importance as a contribution to existing knowledge.

LABORATORY TECHNICAL REPORTS (LTR): Information receiving limited distribution because of preliminary data, security classification, proprietary, or other reasons.

Details on the availability of these publications may be obtained from:

Publications Section,
National Research Council Canada,
National Aeronautical Establishment,
Bldg. M-16, Room 204,
Montreal Road,
Ottawa, Ontario
K1A 0R6

ÉTABLISSEMENT AÉRONAUTIQUE NATIONAL

PUBLICATIONS SCIENTIFIQUES ET TECHNIQUES

RAPPORTS D'AÉRONAUTIQUE

Rapports d'aéronautique (LR): Informations scientifiques et techniques touchant l'aéronautique jugées importantes, complètes et durables en termes de contribution aux connaissances actuelles.

Rapports de génie mécanique (MS): Informations scientifiques et techniques sur la recherche externe à l'aéronautique jugées importantes, complètes et durables en termes de contribution aux connaissances actuelles.

CAHIERS D'AÉRONAUTIQUE (AN): Informations de moindre portée mais importantes en termes d'accroissement des connaissances.

RAPPORTS TECHNIQUES DE LABORATOIRE (LTR): Informations peu disséminées pour des raisons d'usage secret, de droit de propriété ou autres ou parce qu'elles constituent des données préliminaires.

Les publications ci-dessus peuvent être obtenues à l'adresse suivante:

Section des publications
Conseil national de recherches Canada
Établissement aéronautique national
Im. M-16, pièce 204
Chemin de Montréal
Ottawa (Ontario)
K1A 0R6

UNLIMITED
UNCLASSIFIED

ANALYSIS OF EXPERIMENTAL DATA FOR CAST 10-2/DOA2 SUPERCRITICAL AIRFOIL AT HIGH REYNOLDS NUMBERS

ANALYSE DE DONNÉES EXPÉRIMENTALES POUR LE PLAN SUPERCRITIQUE CAST 10-2/DOA2 EN FONCTION DE NOMBRES DE REYNOLDS ÉLEVÉS

by/par

Y.Y. Chan

National Aeronautical Establishment

AERONAUTICAL NOTE
NAE-AN-49
NRC NO. 28595

OTTAWA
JANUARY 1988

L.H. Ohman, Head/Chef
High Speed Aerodynamics Laboratory/
Laboratoire d'aérodynamique à hautes vitesses

G.F. Marsters
Director/Directeur

SUMMARY

Experimental data obtained in the NAE Two-Dimensional Test Facility for CAST 10-2/DOA2 supercritical airfoil have been analyzed for the effects of Reynolds number, transition fixing and Mach number. The data were obtained for Reynolds numbers from 6 to 30 million and Mach numbers from 0.3 to 0.8 with fixed and free transitions. The analysis indicates that the aerodynamic parameters of the airfoil depend strongly on Reynolds number and transition fixing. Above Reynolds number 10 million the trends of dependency on Reynolds number with free or fixed transition can be established. For lower Reynolds number, the long stretch of laminar boundary layer over the airfoil alters the flow characteristics significantly and the data do not follow the trends for high Reynolds numbers.

RÉSUMÉ

Des données expérimentales obtenues dans la veine d'essai bidimensionnelle de l'ÉAN pour le plan aérodynamique supercritique CAST 10-2/DOA2 *ont été* analysées les effets du nombre de Reynolds, de la détermination du point de transition et du nombre de Mach. Pour des points de transition fixes et aléatoires, on a obtenu des nombres de Reynolds compris entre 6 et 30 millions, et des nombres de Mach compris entre 0,3 et 0,8. L'analyse révèle que les paramètres aérodynamiques du plan dépendent en très grande partie du nombre de Reynolds et de la détermination du point de transition. Au-dessus d'une valeur de dix millions, on peut dégager les tendances de la relation entre le nombre de Reynolds et un point de transition fixe ou aléatoire. Pour les nombres de Reynolds inférieurs à cette valeur, la longue couche limite laminaire sur le plan aérodynamique modifie considérablement les caractéristiques de l'écoulement, et alors les données ne suivent pas les tendances observées pour les nombres de Reynolds élevés.

TABLE OF CONTENTS

		Page
	SUMMARY	(iii)
	LIST OF FIGURES	(v)
	SYMBOLS	(viii)
1.	INTRODUCTION	1
2.	ENVELOPE OF EXPERIMENTAL CONDITIONS	2
3.	BOUNDARY LAYER TRANSITION	3
4.	TWO-DIMENSIONALITY OF FLOW OVER MODEL	4
5.	REYNOLDS NUMBER EFFECTS	5
	5.1 Lift, Pitching Moment and Drag	6
	5.2 Shock Location and Shock Mach Number	10
	5.3 Trailing Edge Pressure	13
6.	MACH NUMBER EFFECTS	13
7.	CONCLUSIONS	17
	REFERENCES	20

LIST OF FIGURES

		Page
1.	Section Profile of CAST 10-2/DOA 2 Airfoil	23
2.	Envelope of test conditions	24
3.	Effects of Reynolds number, Mach number and incidence on locations of boundary layer transition on the upper surface of the model	25
4.	Spanwise wake drag variations at various Reynolds numbers for two angles of attack with fixed or free transition, M_∞ = 0.765	26
5.	Spanwise pressure distributions at x/c = 0.9 for two angles of attack at various Reynolds numbers with fixed or free transition, M_∞ = 0.765	27
6a	Lift versus angle of attack at various Reynolds numbers with fixed or free transition at nominal M_∞ = 0.765	28
6b	Pitching moment versus lift at various Reynolds numbers with fixed or free transition at nominal M_∞ = 0.765	29
6c	Drag versus lift at various Reynolds numbers with fixed or free transition at nominal M_∞ = 0.765	30
6d	Reynolds number dependence of lift for two angles of attack with fixed or free transition	31
6e	Reynolds number dependence of drag for two angles of attack with fixed or free transition	32
7a	Reynolds number effects on surface pressure distributions at nominal $\alpha = 1.35^\circ$, M_∞ = 0.765. The first two cases are with transition fixed, the rest are transition free	33
7b	Reynolds number effects on surface pressure distributions at nominal $\alpha = 3.25^\circ$, M_∞ = 0.765. The first two cases are with transition fixed, the rest are transition free	34

LIST OF FIGURES (Cont'd)

		Page
8a	Wake profiles showing laminar and turbulent boundary layer shock-wave interactions respectively at $M_\infty = 0.765$, $\alpha = 1.35°$	35
8b	Wake profiles showing laminar and turbulent boundary layer shock-wave interactions respectively at $M_\infty = 0.765$, $\alpha = 1.75°$	36
9	Surface pressure distributions at different angles of attack at nominal $M_\infty = 0.765$, $R_{e_c} = 30\times10^6$, transition free	37
10a	Shock location versus angle of attack at various Reynolds numbers with fixed or free transition at nominal $M_\infty = 0.765$	38
10b	Shock location versus lift at various Reynolds numbers with fixed or free transition at nominal $M_\infty = 0.765$	39
10c	Reynolds number dependence of shock location for two angles of attack with fixed or free transition	40
11a	Shock Mach number versus angle of attack at various Reynolds numbers with fixed or free transition at nominal $M_\infty = 0.765$	41
11b	Shock Mach number versus lift at various Reynolds numbers with fixed or free transition at nominal $M_\infty = 0.765$	42
11c	Reynolds number dependence of shock Mach number for two angles of attack with fixed or free transition	43
12a	Trailing edge pressure versus angle of attack at various Reynolds numbers with fixed or free transition at nominal $M_\infty = 0.765$	44
12b	Trailing edge pressure versus lift at various Reynolds numbers with fixed or free transition at nominal $M_\infty = 0.765$	45
12c	Reynolds number dependency of trailing edge pressure for two angles of attack with fixed and free transition	46
13a	Lift versus angle of attack at various Mach numbers at nominal $R_{e_c} = 30\times10^6$ with free transition	47
13b	Pitching moment versus lift at various Mach numbers at nominal $R_{e_c} = 30\times10^6$ with free transition	48

LIST OF FIGURES (Cont'd)

		Page
13c	Drag versus lift at various Mach numbers at nominal $R_{e_c} = 30\times10^6$ with free transition	49
14	Lift curve slope at zero lift versus Mach numbers at various Reynolds numbers with fixed or free transition	50
15a	Maximum lift versus Mach number at various Reynolds numbers with fixed or free transition	51
15b	Reynolds number dependence of maximum lift at various Mach numbers with fixed or free transition	52
16a	Mach number effects on surface pressure distributions at nominal α = 1.35°, $R_{e_c} = 20\times10^6$ with fixed transition	53
16b	Mach number effects on surface pressure distribution at nominal α = 3.35°, $R_{e_c} = 20\times10^6$ with fixed transition	54
17a	Mach number and Reynolds number dependence of lift at two angles of attack with fixed transition	55
17b	Mach number and Reynolds number dependence of drag at two angles of attack with fixed transition	56
18	Minimum drag versus mach number at various Reynolds numbers with fixed or free transition	57
19	Drag at $C_L = 0.6$ versus Mach number at various Reynolds numbers with fixed or free transition	58
20	Reynolds number dependence of drag at $M_\infty = 0.765$, $C_{L_p} = 0.5, 0.6$ with fixed or free transition	59
21	Reynolds number dependence of drag rise Mach number for two lift conditions with fixed and free transition	60

LIST OF SYMBOLS

Symbol	Definition
b	tunnel width, model span
c	chord length
C_{D_W}	drag coefficient, wake integration
$C_{D_{min}}$	minimum drag coefficient
$C_{L_{max}}$	maximum lift coefficient
C_{L_p}	lift coefficient, pressure integration
C_{L_α}	lift curve slope
$C_{m_{c/4}}$	pitching moment coefficient, quarter chord
C_p	pressure coefficient
$C_{p_{T.E.}}$	pressure coefficient, trailing edge
CDW2	local wake drag coefficient, probe 2 at 2y/b = 0.233 from centre-line
M_∞	free stream Mach number
M_D	drag rise Mach number
M_s	shock Mach number
R_{e_c}	free stream Reynolds number based on chord length
V_s	side-wall suction velocity
U	free stream velocity
x,y,z	Cartesian coordinates, x in chordwise direction
x_s	shock position on model
x_t	transition location
α	angle of attack

1. INTRODUCTION

The NAE/NRC-NASA Langley Cooperative Program on Two-Dimensional Wind Tunnel Wall Interference Research was initiated in 1984. The objective of the program is to develop the technology for elimination or correction of wall interference in transonic two-dimensional tests using the Langley 0.3 m. Transonic Cryogenic Tunnel with an adaptive wall test section and the NAE 1.5 m High Reynolds Number Two-Dimensional Test Facility. A common model with the CAST 10-2/DOA 2 profile and 228 mm (9 inches) chord length has been tested in both tunnels. The profile of the airfoil is shown in Fig. 1. By comparing the test data from these two tunnels the techniques of elimination or correction of wall interference in the corresponding facilities can be critically evaluated. The tests performed in NAE covered the Mach numbers from 0.3 to 0.8 and Reynolds number from 10 to 30 million. One case at low Reynolds number of 6 million was also run at the design Mach number of 0.765. The model was tested with transition free and with transition fixed at 5 percent chord for both the upper and the lower surfaces. These data have, aside from the original purpose for wall interfrerence studies, unique value in that they provide an opportunity for direct comparison of transonic testing data with and without transition fixing for a wide range of Reynolds number and Mach number.

It is well known that the development of the boundary layer over a transonic airfoil has a strong influence to its performance. It affects the effective shape of the airfoil, the characteristics of the interaction with the shock wave and the trailing edge separation. Therefore an airfoil with and without transition fixing will not give the same

performance even at the same Reynolds number and Mach number. The present data, with both transition free and fixed, will allow us to investigate in detail of the difference of the flows at these conditions. The highest Reynolds number of 30 million in the testing is approaching the flight Reynolds number of a large transport aircraft. These data of high Reynolds number can thus be considered as asymptotes for comparison with the other data obtained at lower Reynolds numbers and for establishing the data trends for Reynolds number variation. The results of the analysis will help us to select the test conditions for proper simulation of the flight condition and to interpret the test data for airfoil development programs in the future.

In computational aerodynamics, the accuracy of the computational code is usually assessed by comparing the results with experimental data with emphasis on some parameters such as lift, drag, shock conditions and trailing edge separation. The present analysis shows that all these parameters are sensitive to Reynolds number and the transitional condition of the boundary layer. Therefore for proper assessment of the computational method, the test data must be chosen with great care and with special attention to the aforementioned conditions.

2. ENVELOPE OF EXPERIMENTAL CONDITIONS

In the first phase (phase I) of the program the airfoil was tested with transition fixed at 5% chord at the upper and the lower surfaces at Reynolds numbers 10, 15 and 20 million and at Mach numbers of 0.3 to 0.8. The test envelope is shown in Fig. 2. In the second phase

(phase II), the airfoil was tested with free transition for the same test envelope. Additional tests were performed at Reynolds number 30 million in the transonic range of Mach Numbers 0.7 to 0.79. A low Reynolds Number run of 6 million at the design Mach number 0.765 was also carried out. The results of the phase I and II - investigations have been fully reported in References 1 and 2 respectively.

3. BOUNDARY LAYER TRANSITION

In phase II of the program, investigations have been carried out to determine the location of the boundary layer transition at the upper surface of the airfoil and its dependency on Reynolds number, Mach number and angle of attack. The results are shown in Fig. 3. This information is essential for the analysis of the experimental data presented in the following sections. At a constant Mach number, the transition position moves forward as Reynolds number increases, with transition Reynolds number remaining at about 2 million. For a fixed Reynolds number the transition position is only slightly affected by Mach number indicating that the compressibility effect is small in the transonic range. With both Mach and Reynolds numbers fixed the transition location varies with angles of attack. The downstream movement of the transition location as the incidence increases is caused by the unique characteristics of the pressure distribution at the forward portion of the supercritical airfoil. Following the leading edge expansion, the supersonic flow produces a constant pressure plateau until terminated by a shock wave. The expansion and the constant pressure flow both provide favourable conditions for the laminar boundary layer stability. At low Reynolds numbers, the laminar

flow may extend to 50% chord length even at angles of attack up to 4 degrees.

4. TWO-DIMENSIONALITY OF FLOW OVER MODEL

The uniformity of the flow across the span of the model in the test section is maintained by side wall boundary layer control. The two-dimensionality of the flow can be confirmed by inspecting the spanwise variation of the flow quantities such as wake drag or surface pressure distributions. Figure 4 shows the drag variation obtained from integrating the wake profiles traversed at four stations along the span of the model. At moderate angles of attack, the spanwise uniformity is established for cases with fixed transition. With free transition, the slight irregularity observed is a direct consequency of the spanwise variation of the transition location. At the centre plane of the model, the disturbances generated by the pressure taps induce early transition, hence a thicker wake profile and higher drag are observed at this station. This is clearly shown in the figure for the free transition case with Reynolds number 10 million. Drag at the centre-line is very close to the other cases with fixed transition while the values at other stations are lower due to the long stretch of laminar boundary layer at the forward portion of the model. At Reynolds number 20 million, the transition moves forward and the resulting drag variation is very much the same as that with fixed transition.

At high angles of attack with flow separation at the rear of the airfoil, drag varies greatly across the span. Drag is highest at the central plane and drops off to about a half of the value as the side wall

is approached. This indicates that the separation is largely confined at the central region of the airfoil in a form of a laterally elongated bubble. Near the side wall, the severity of separation may have been reduced by the vortical flow generated at the wing-wall junction. The transition free case at low Reynolds number again exaggerates the drag variation. However, the general trend of the drag tends to approach that of the transition fixed as Reynolds number becomes large.

The spanwise flow uniformity can also be observed from the spanwise pressure distribution as shown in Figure 5. There are 3 spanwise pressure taps at 90% chord at each side of the central measuring station. At low angles of attack or moderate lift coefficients two-dimensionality of flow is shown to be well established. At high angles of attack, well into stall, large variation of pressure can be observed at the upper surface. For transition fixed cases a low pressure separation zone at the central portion of the model is shown. The pressure distribution is nearly symmetrical with respect to the central plane. With transition free, however, the flow is highly asymmetric especially for the low Reynolds number case. This is primarily due to the spanwise variation of the transition location which affects the downstream boundary layer development and its resistance to separation. At high Reynolds number, the transition free case is again approaching the transition fixed case.

5. REYNOLDS NUMBER EFFECTS

At transonic speeds the flow past an airfoil is extremely sensitive to the slightest variation of the airfoil contour. The displacement thickness of the boundary layer over the airfoil effectively

modifies its profile and hence its performance. Thus a transonic airfoil is highly sensitive to boundary layer development and consequently the free stream Reynolds number. The Reynolds number effects on the model are analysed in some detail with the case at Mach number of 0.765, the design Mach number of the airfoil, as an example. The results of the analysis can be applied, in principle, to other cases within the transonic range.

5.1 Lift, Pitching Moment and Drag

The lift versus angle of attack curves for both transition free and fixed are shown in Figure 6a. The transition fixed cases covering Reynolds numbers 10 to 20 million are first analysed. The lift curves are nearly parallel to each other and shift upwards as Reynolds number increases. The displacement effect causes a reduction of camber of the airfoil, thus, as the boundary layer thickness decreases at high Reynolds number, the geometric camber is approached and higher lift is obtained. The linear portion of the lift curve extends up to about 1 degree and nonlinear lift develops thereafter. The nonlinear contribution to lift is attributed to the extension of the supercritical flow towards the rear part of the airfoil. The maximum lift, about 0.7, occurs at about 2.3 degrees. At about 3 degrees, the trailing edge separation extends upstream to the shock. These flow properties are also shown in the pitching moment variations, Figure 6b. The negative moment increases with the reduction of the displacement effect. The downstream extent of the supercritical flow causes a steady drop of the moment until the onset of separation. The drag polars are shown in Figure 6c. The drag divergency occurs at lift coefficient about 0.55 when the wave drag induced by the shock wave becomes appreciable. The drag before the drag divergency

contains mainly the skin friction drag and thus decreases as Reynolds number increases. The performance of the case at Reynolds number 20 million is very close to that with free transition at Reynolds number 30 million, which has a transition location at about 5% chord estimated from the transition data shown in Figure 3. This indicates that the roughness trip for the present cases is correctly designed with negligible trip drag and without excessively thickening the boundary layers.

The Reynolds number dependency of lift is shown by cross-plotting the lift coefficients at fixed angles of attack, Figure 6d. The nominal value of 1.35 degrees is about the design lift condition and the 3.35 degree is beyond the maximum lift condition with separation occurring at the near portion of the airfoil. For fixed transition, the trend with Reynolds number is well defined and the empirical correlation established may be applied for extrapolation to higher Reynolds number. A cross-plotting for drag is given in Figure 6e and again the data is well correlated to Reynolds number. The corresponding surface pressure distributions for these data points are shown in Figures 7a and 7b.

The lift versus angle of attack curves for transition free cases are also shown in Fig. 6a for Reynolds numbers 6 to 30 million. The case of Reynolds number 30 million is particular important as its value is close to the flight Reynolds number of a large transport aircraft. For this case, the transition location is estimated from Figure 3 to be at 5% chord. The lift curve is very close to that with fixed transition at Reynolds number 20 million. At Reynolds numbers of 20 and 15 million, the lift and the pitching moment curves follow those of the 30 million case closely. This behaviour of near independency of Reynolds number indicates

that the turbulent boundary layer characteristics do not change appreciably over the range of Reynolds number. This is due to the fact that the thickening of the turbulent boundary layer at low Reynolds number is compensated by the shortening of the turbulent boundary layer development length, as the transition location shifts downstream. For profile drag shortening the turbulent wetted area contributes directly to lower the drag value.

At Reynolds number 6 million, a significant change of flow characteristics can be observed. The lift curve remains linear up to zero degree incidence and then becomes nonlinear but with reduction of slope. The first peak of lift is reached at 2.25 degrees incidence and a second peak at 4 degrees. These deviation of flow pattern from the other high Reynolds number cases are due to the large extent of laminar boundary layer flow as far back to 40 to 50 percent chord. The long stretch of laminar boundary layer reduces the displacement effect and its modification of the airfoil camber, giving a slightly higher lift at low angles of attack. At high angles of attack, the laminar flow remains and interacts with the shock wave. This can be identified by the surface pressure distribution, Figure 7a, at the interaction region with a slight compression before the shock followed by a weak expansion after the interaction[3,4]. The laminar or the turbulent nature of the boundary layer can also be detected from the thicknesses of the wake profiles as shown in Figure 8a. The distinction between the laminar and the turbulent interaction with the shock wave is even more pronounced in Figure 8b. At higher angles of attack, the shock-laminar boundary layer interaction induces a local separation which produces the first "bend" of the lift

curve. The separation, however, does not extend to the trailing edge, as indicated by the positive trailing edge pressure (see Figure 7b). With further increases in the angle of attack, the shock induced separation merges with the trailing edge separation and the second bend of the lift curve is formed (See Figure 6a). The delay of the trailing edge separation is due to the fact that the thin turbulent boundary layer is less prone to separate at the adverse pressure conditions. These low Reynolds number flow characteristics are also shown in the pitching moment variation which is quite different from the other cases especially at the high lift region (Figure 6b). These analyses are in good agreement with those of the low Reynolds number (2.35 million) tests reported in Reference 5. The profile drag is necessarily low because of the large extent of the laminar boundary layer. The "drag bucket" formed before the drag divergency is also due to the long stretch of laminar flow which may extend to 60% chord at the design lift of 0.6[6](Figure 6c). Because of the delay of the trailing edge separation, the drag rises less sharply at the high lift condition and the maximum lift coefficient reaches a value of 0.8, about 0.1 greater than the other cases.

The Reynolds number dependency shown in Figure 6d and 6e show distinct characteristics for data above and below 10 million. However, if the low Reynolds number case is excluded, a near linear dependency on Reynolds number can be established for the data at 10 million and higher. These correlation curves can also be used for extrapolation to higher Reynolds number.

5.2 Shock Location and Shock Mach Number

The supersonic flow over the transonic airfoil terminates at a shock wave through which the flow is recompressed to subsonic speeds. The interaction of the shock wave with the boundary layer alters the local and downstream flow conditions. A severe interaction may cause the flow to separate and greatly inhibit the performance of the airfoil. The effects of transition fixing and Reynolds number on the formation of the shock are examined as follows.

The typical variations of the shock position and the shock strength can be qualitatively observed from the pressure distribution plots as shown in Figure 9. The shock position is defined as the location at which the shock Mach number equal to 1.1[7]. Figure 10a shows the shock positions for a range of Reynolds numbers with free and fixed transition. For free transition at low angles of attack, the shock is nearly stationary until about 1 degree. As the angle of attack increases, the shock moves forward rapidly for a distance of five percent chord and than stabilizes again until the onset of the trailing edge separation at about 2 degrees. A steady forward shift takes place as the separation develops. For the transition free cases the Reynolds number effect for 10 to 30 million is small because of the compensation of the growth of the boundary layer by the movement of transition as discussed in the preceding section. The case with Reynolds number 6 million follows the general trend of the other cases until about 1 degree incidence. The forward shift at the higher angles of attack is about eight percent chord and remains stable up to the highest angle of attack, although a forward shift trend is discernible, indicative of approaching onset of trailing edge separation.

For the transition fixed cases, the shift of the shock locations is because of the effective change of the airfoil camber by the displacement effect of the boundary layer. For the case with Reynolds number 10 million, the shock locates more forward, about three to four percent chord than the transition free cases at low incidences. This difference diminishes as Reynolds number is increased to 20 million, with the consequent reduction in boundary layer thickness. At the onset of the trailing edge separation the shock position becomes less sensitive to Reynolds number, with or without transition fixing.

In Figure 10b the shock positions are plotted against lift coefficient. Before the onset of separation the data behave very much the same as those in Figure 10a since the lift is largely linearly related to the angle of attack. Once the maximum lift is reached, however, the shock moves rapidly upstream while the lift remains nearly constant. The movement is nearly independent of Reynolds number. The cross-plots at fixed angle of attack, Figure 10c, show again that the low Reynolds number case of 6 million stands out from the other data, particularly the high incidence case. The reason is that the flow is attached at low Reynolds number while separated at the higher Reynolds numbers. At moderate incidence, the transition fixed cases show a downstream movement of the shock position as Reynolds number increases while the transition free cases show the shock is practically stationary. For high incidences the trends for the transition free and fixed cases are reversed. This dependency of Reynolds number can also be seen from the pressure distributions as shown in Figures 7a and 7b.

The shock Mach number, defined as the value before the sudden drop of the local flow Mach number at the airfoil surface, is shown in Figure 11a as a function of angle of attack. With transition free, the shock Mach number is only weakly dependent on Reynolds number. At low angles of attack, the small supersonic bubble located from about 40% to 70% chord generates a weak shock, the shock Mach number increasing with incidence. As incidence gradually increases the weak shock remains at constant strength for a short while until the rear supersonic flow pocket merges with the rapidly expanding forward supercritical flow (See Figure 9). The shock strength then increases rapidly with incidence. At and after the onset of the trailing edge separation the rate of growth of the shock strength reduces abruptly as the leading edge expansion slows down with increasing incidence. The low Reynolds number case of 6 million follows the general trend well but then deviates from the others at high incidences because of its delay in separation. With transition fixed, the shock Mach number are lower at low incidences. This may be caused by the thicker turbulent boundary layer reducing the upper surface expansion and hence the shock strength. At higher angles of attack, the displacement effect diminishes and the data follow the other cases closely. The data are replotted against lift coefficient in Figure 11b. The deviation of the low Reynolds number case is more pronounced than in Figure 11a. The cross-plots at fixed angles of attack, Figure 10c, show that the shock Mach number is nearly independent of Reynolds number for 10 million and higher. For the transition fixed cases at low angles of attack, the lower values are again due to boundary layer displacement effects.

5.3 Trailing Edge Pressure

The measured trailing edge pressure provides an excellent indication of trailing edge separation and its development. The trailing edge pressure coefficient versus angles of attack is shown in Figure 12a. Generally, the trailing edge pressure coefficient decreases slowly with increasing incidence up to about 2 degrees, after which it drops rapidly, a clear indication of trailing edge separation. The transition fixed cases show slightly lower values due to the thicker boundary layer. The case with Reynolds number 6 million and free transition again stands out because of the delayed separation due to thinner boundary layer. The data are plotted against the lift coefficient in Figure 12b. Before the onset of separation the trailing edge pressure is not constant as expected but decreases gradually as the boundary layer thickens. It then drops abruptly at nearly constant lift as separation sets in. The cross-plots at fixed angles of attack. Figure 12c, show a general trend with Reynolds number. At high incidences with separation extending to the shock, the Reynolds number dependence becomes less regular as the interaction with the shock makes the flow more complicated.

6. MACH NUMBER EFFECTS

The experiments were performed for Mach numbers from 0.3 to 0.8. The low Mach number tests were conducted to provide data for the applied correction method for wind tunnel wall interference at subcritical flow conditions[8]. The correction method gives the first order corrections, which are exact for subcritical flows, to the measurements in transonic flows[9]. The corrected low Mach number data should thus provide exact

test cases for comparison with theory. This data, however, will not be discussed herein, since the transonic performance is emphasized in the present analysis. In passing, however, it is noted that at Mach number 0.3, the airfoil behaves like a typical low speed airfoil, having a peaky leading edge suction followed by a gradual compression over the rest of the profile. The lift curve is linear up to 8 degrees angle of attack. At higher Mach number of 0.5 and 0.6, a small pocket of supersonic flow develops from the leading edge extending to a few percent chord downstream. A weak shock terminates the supersonic flow and a gradual recompression follows for the rest of the airfoils. At this Mach number range, the flow over the airfoil is mainly subsonic and is not so sensitive to the boundary layer displacement effect. Thus the dependency of Reynolds number is small.

At the transonic range of Mach number 0.7 to 0.8, the lift coefficient versus angles of attack is shown in Fig. 13a while pitching moment and drag coefficients are shown in Figures 13b and 13c respectively for Reynolds number 30 million. The lift curve slope increases with Mach number while the maximum lift coefficient decreases. The pitching moment becomes more negative as the rear loading increases due to the downstream extension of the supersonic flow pocket over the upper surface of the airfoil. The growth of the shock strength induces a rapid increment of drag, especially for Mach number higher than the design value of 0.765.

The slope of the linear portion of the lift curve is plotted against Mach number in Fig. 14 for the Mach number and Reynolds number ranges covered in the experiment. The slope increases steadily with Mach number, steepening after Mach number 0.7 and reaching a peak at Mach

number 0.78. At higher Mach number, the strong shock induces separation even at relatively low angle of attack, causing a sharp drop of the lift curve slope. The strong influence of Reynolds number and the boundary layer transition fixing conditions are also shown in the figure. With transition free, a difference of ten percent in the slope can be observed for Reynolds numbers from 10 to 20 million. Above 20 million, the increment becomes very small. With fixed transition the slope also increases with Reynolds number. The Reynolds number effect for the latter case, however, is much less pronounced.

The maximum lift coefficient for the transonic range is shown in Fig. 15a. The value drops rapidly as Mach number increases. This is caused by separation induced by a strong shock at high incidences. The maximum lift coefficient increases with Reynolds number as the boundary layer becomes thinner. The cross-plots of Reynolds number dependency for cases at different Mach numbers are shown in Fig. 15b. With free transition, the value tends to drop slightly from Reynolds number 10 to 20 million and then reaches a higher value at 30 million. With fixed transition, the value increases steadily with Reynolds number and the extrapolation of the trend to higher Reynolds number gives a value very close to that of free transition at 30 million.

The evolution of the pressure distribution at the airfoil as Mach number increases from subsonic to transonic is shown in Figs. 16a and 16b at Reynolds number 20 million for fixed angles of attack. In Fig. 16a, the development of the supersonic flow and the "roof top" pressure plateau is clearly illustrated. At higher angles of attack, Fig. 16b, the transition from the smooth subsonic recompression to the shock induced

separation at the rear portion of the airfoil is also well demonstrated. The aerodynamic parameters of these cases are cross- plotted in Figs. 17a and 17b. The lift coefficient is shown in Fig. 17a with data from two Reynolds numbers, 10 and 20 million. At low angles of attack the lift peaks at the design Mach number 0.765 and reaches the design value of 0.6 at Reynolds number 20 million. The trend of the Reynolds number effect is similar to that of the lift curve slope discussed previously. Variations of drag with Mach number are shown in Fig. 17b. At low angle of attack, the drag curve turns sharply upward at the design Mach number because of the rapid increase of wave drag. At high angles of attack, the drag rise before Mach number about 0.65 is mainly due to wave drag. At higher Mach number the shock induced separation occurs causing further increase in pressure drag. Since these cases are with transition fixed, the Reynolds number effect is small.

Figure 18 shows the variation of minimum drag versus Mach number with and without transition fixing. With fixed transition the lower skin friction at higher Reynolds number contributes to the difference in drag as just discussed. With transition free the drag variation with Mach number depends weakly on Reynolds number because of the shift of the transition location. The long stretch of laminar boundary layer flow at Reynolds number 10 million formed by the favourable conditions at the transonic range reduces the total drag and a "drag bucket" is formed before the drag rise at the design Mach number. This unique low Reynolds number characteristics has led to design studies of low drag transonic airfoil with natural laminar flows[6]. At higher Reynolds number the drag bucket disappears as the transition moves towards the leading edge. At

Reynolds number 30 million, the drag rise curve behaves similarly as those with transition fixed except having a lower value due to lower skin friction.

The drag variations at the design lift condition are shown in Fig. 19. The gradual increment of drag with Mach number, the drag creep, is caused mainly by wave drag[10]. At the design Mach number the Reynolds number dependency is shown in Fig. 20. With fixed transition the negative slope reflects the decrease of the skin friction as Reynolds number increases and with transition free the positive slope indicates lengthening the surface wetted by the turbulent boundary layer. Both cases approach the same drag value at very high Reynolds number as expected. The drag rise Mach number, defined as the point at the drag rise curve having a slope of 0.1, is shown in Fig. 21 for two values of lift. A weak dependency on Reynolds number and transition conditions can be detected. For lift coefficient 0.5, the drag rise Mach number is close to the design value of 0.765 for both fixed and free transition.

7.0 CONCLUSIONS

The experimental data obtained in the NAE Two-Dimensional Test Facility for the CAST 10-2/DOA2 model have been analysed for the effects of Reynolds number, transition fixing and Mach number. The role of the boundary layer on the displacement effect, the interaction with the shock wave and the trailing edge separation are examined. The results of the analysis are summarized as follows.

1. The airfoil performance depends strongly on Reynolds number and transition fixing.

2. With transition fixed near the leading edge, the aerodynamic quantities such as lift, pitching moment and drag show a monotonic variation with Reynolds number. Extrapolation to higher parametric values are believed reliable.
3. With transition free, the aerodynamic quantities vary irregularly with Reynolds number. For Reynolds number 10 million and above, a slight parametric dependency is shown. The weak effect is due to the compensatory effect of the forward shift of the transition and the thinning of the turbulent boundary layer as Reynolds number increases.
4. For Reynolds number 6 million and free transition, the aerodynamic quantities deviate appreciably from those of higher Reynolds numbers. This is caused by the long stretch of laminar boundary layer flow and the different characteristics of the shock-laminar boundary layer interaction. The turbulent boundary layer originating from the interaction is so thin over the rear part of the airfoil that the trailing edge separation is appreciably delayed. The data do not follow the trend established for the high Reynolds numbers.
5. Excluding the low Reynolds number case, the shock Mach number and the shock position are only weakly dependent on Reynolds number. If transition fixing is applied, the shock Mach number is lower at low angles of attack, the shock position is more forward up to the onset of separation.
6. The long extent of the laminar boundary layer at transonic speeds reduces the drag appreciably at low Reynolds number. The drag bucket around the design Mach number can be observed below Reynolds number 15 million.

7. For transonic airfoil testing for a large transport aircraft, it is preferable to perform at or above Reynolds number 10 million with or without transition fixation. Below this Reynolds number, methods for treating low Reynolds number testing such as aft-fixing must be applied for proper flow simulation[11].

8. When using experimental data for verification of computational aerodynamics codes, the transition location, whether fixed or free must be considered as essential input parameter for the computation code, so that the viscous part of the computed flow is correctly simulated.

REFERENCES

1. Chan, Y.Y. — Wind Tunnel Investigation of CAST 10-2/DOA2 12% Supercritical Airfoil Model. Laboratory Technical Report LTR-HA-5×5/0162. National Research Council Canada, May 1986.

2. Chan, Y.Y. — Wind Tunnel Investigation of CAST 10-2/DOA2 12% Supercritical Airfoil Model, Phase II, Laboratory Technical Report LTR-HA-5×5/0170. National Aeronautical Establishment, National Research Council Canada, June 1987.

3. Mignosi, A. Seraudie, A. Blanchard, A. Breil, J.F. — Premier rapport d'essais du profil CAST 10 (corde = 180 mm) en transition naturelle, effectues dans la soufflerie transsonique cryogenique T2 en presence de parois auto-adaptables. Rapport Technique OA No 59/1685 AND (DERAT No 4/5019 DN). Departement d'etudes et de recherches en aerothermodynamique. O.N.E.R.A. Mars 1985.

4. Delery, J. Marvin, J.G. — Shock-wave Boundary Layer Interactions. AGARD-AG-280, February 1986.

5. Stanewsky, E. — Interaction Between the Outer Inviscid Flow and the Boundary Layer on Transonic Airfoils. Z. Flugwiss. Weltraumforsch. 7 (1983), Heft 4, pp. 242-252.

6. Khalid, M. Jones, S.J. — Further Studies on the 21% Thick, Supercritical NLF Airfoil NAE 68-06-0-21:1. Aeronautical Note NAE-AN-41. National Research Council Canada. September 1986.

7. Lynch, F.T. Bui, M.H. Patel, D.R. — Some Fundamental concepts in the Design Analysis and Testing of Transonic Airfoils. Douglas Paper 7579. McDonnell Douglas Corporation October 1985.

8. Mokry, M. Ohman, L.H. — Application of Fast Fourier Transform to Two-Dimensional Wind Tunnel Wall Interference. Journal of Aircraft, Vol. 17, No. 6, June 1980, pp. 402-408.

9. Chan, Y.Y. — An Asymptotic Analysis of Transonic Wind-Tunnel Interference Based on the Full Potential Theory. Journal of Applied Mathematics and Physics (ZAMP). Vol.36, January 1985, pp. 89-104.

10. Elfstrom, G.M. — Extraction of Wave Drag From Airfoil Wake Measurements. Canadian Aeronautical and Space Journal. Vol. 28, No. 1, March 1982, pp. 42-55.

11. Koppenwallner, G.
Szoduch, J.
(Editors)

Boundary Layer Control by Transition Fixing. DFVLR-Mitt. 84-17, DFVLR Institut für Experimentelle Strömungsmechanik, October 1984.

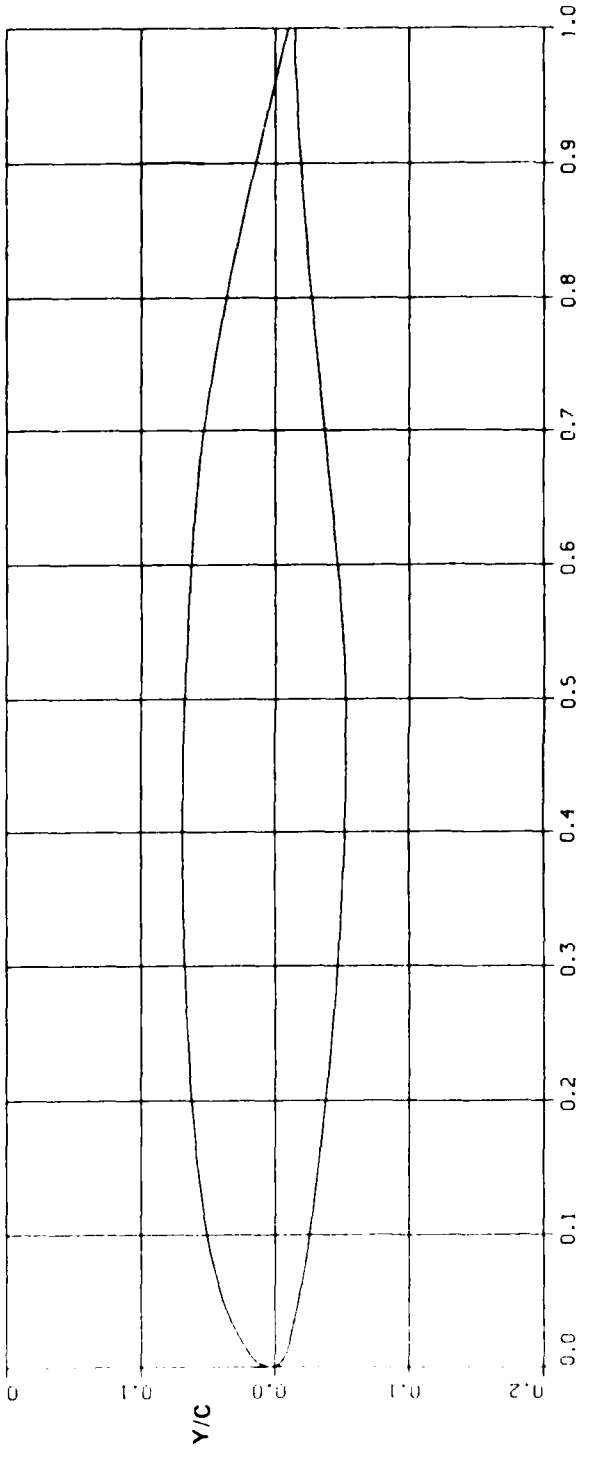

TRAILING EDGE ANGLE (DEG.) 14.83
TRAILING EDGE THICKNESS (%) 0.50

FIG. 1: SECTION PROFILE OF CAST 10-2/D0A 2 AIRFOIL

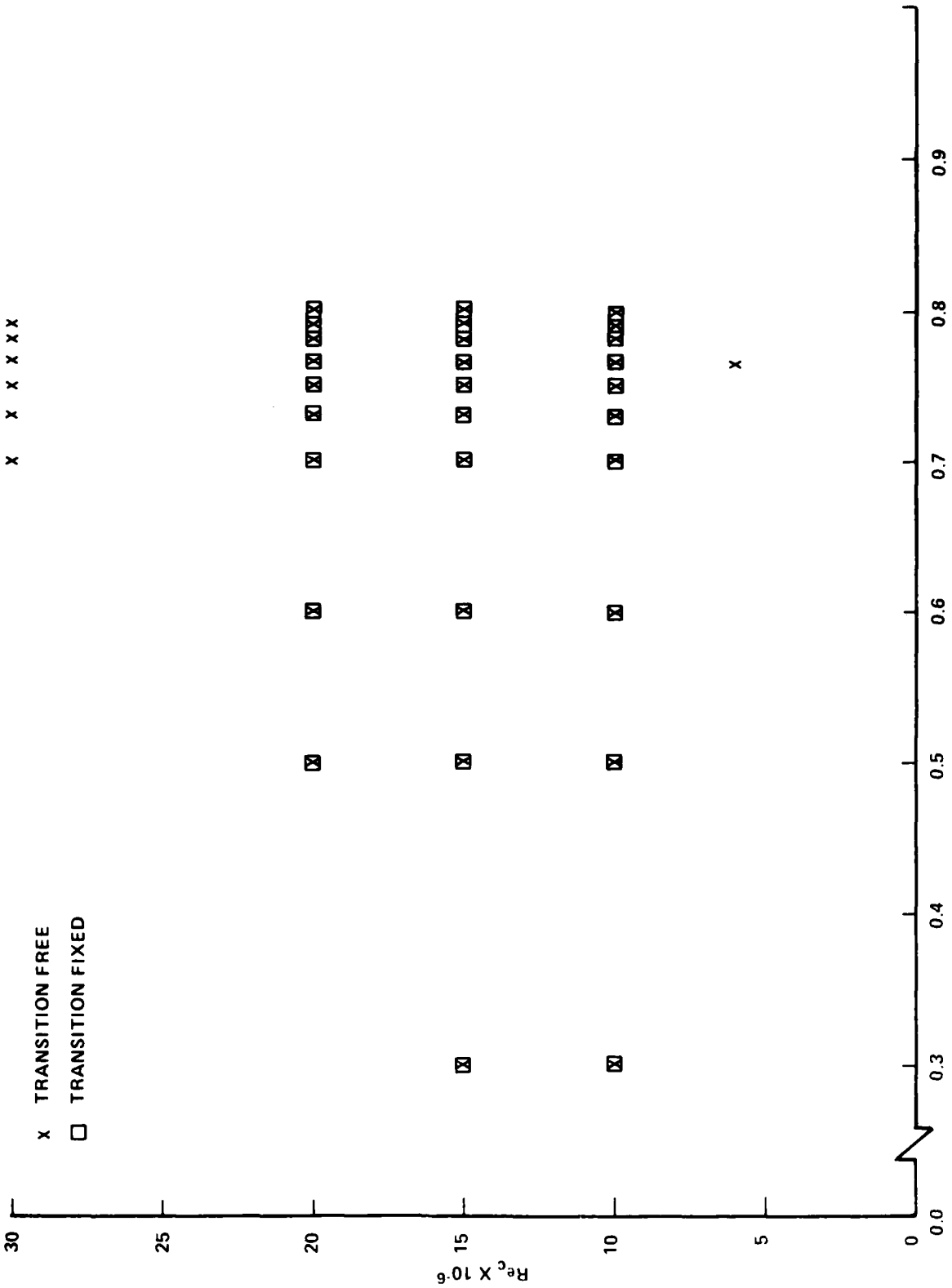

FIG. 2: ENVELOPE OF TEST CONDITIONS

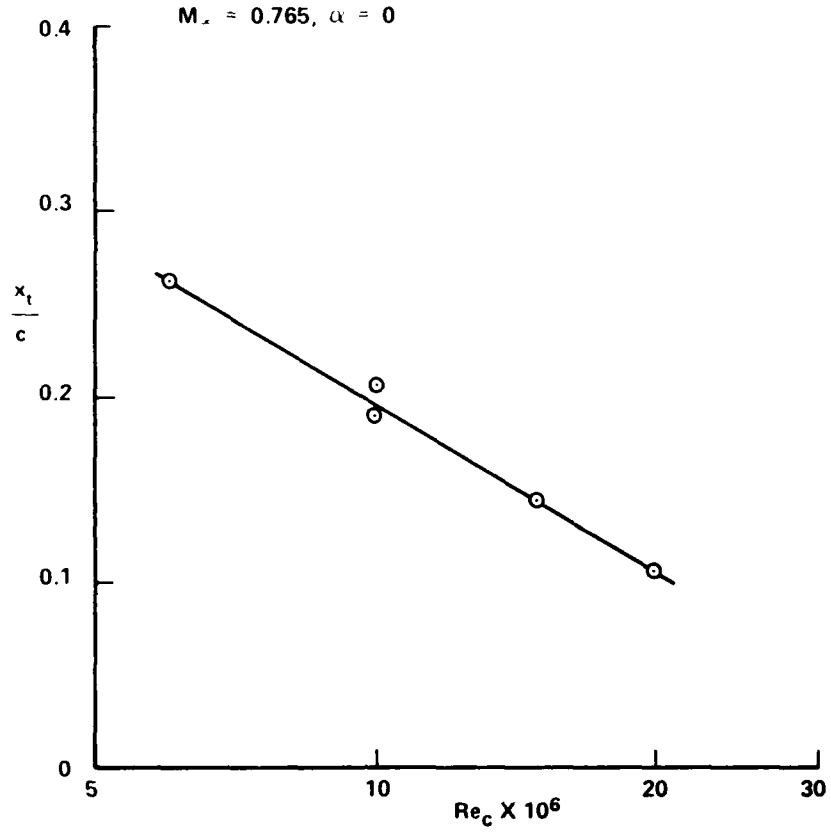

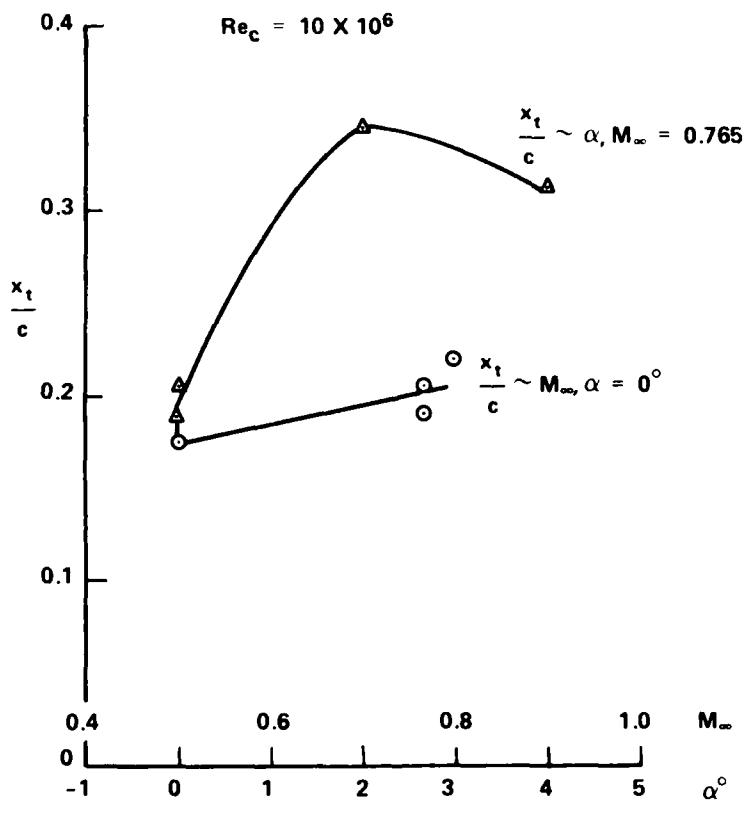

FIG. 3: EFFECTS OF REYNOLDS NUMBER, MACH NUMBER AND INCIDENCE TO LOCATIONS OF BOUNDARY LAYER TRANSITION ON THE UPPER SURFACE OF THE MODEL

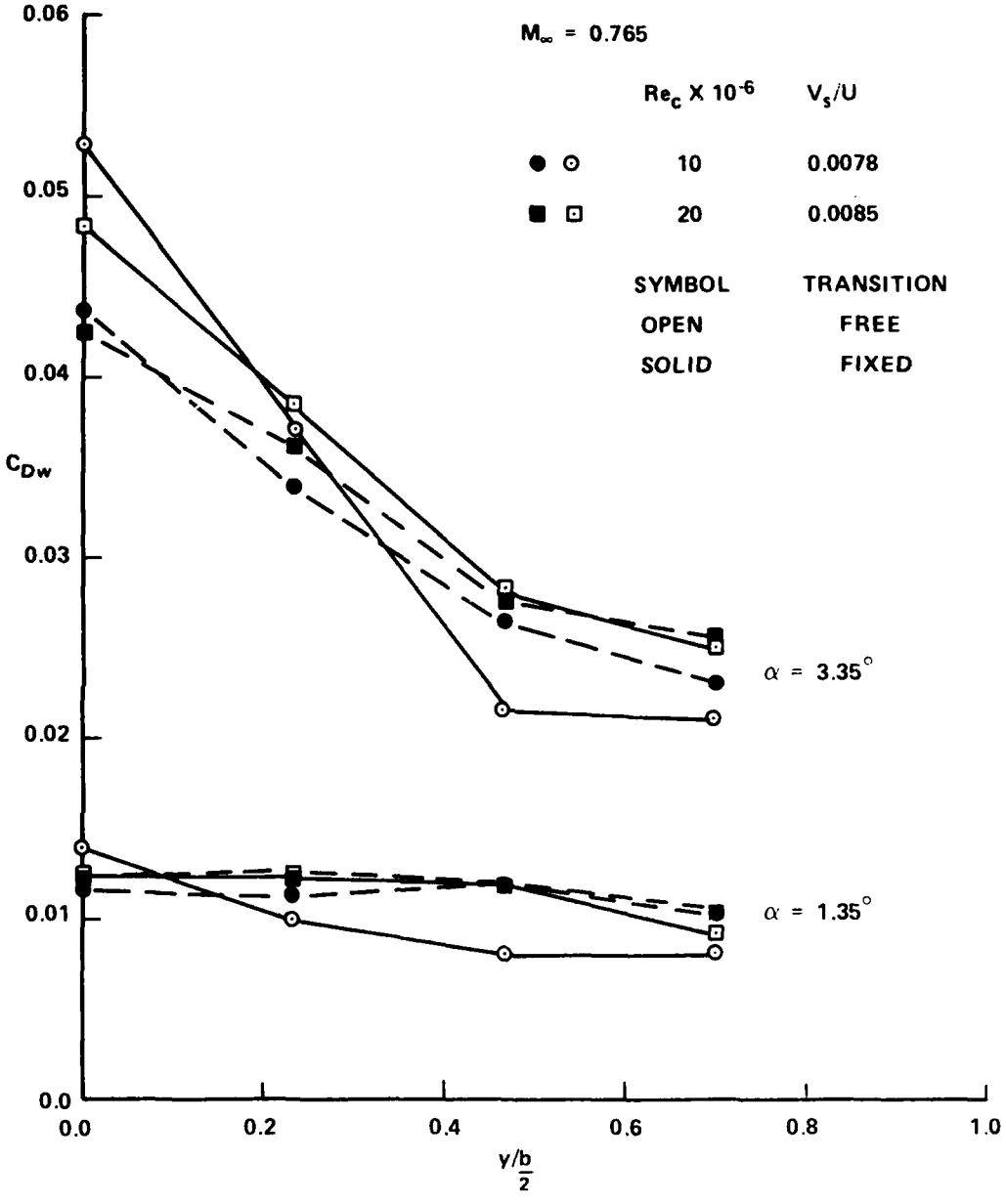

FIG. 4: SPANWISE WAKE DRAG VARIATION AT VARIOUS REYNOLDS NUMBERS FOR TWO ANGLES OF ATTACK WITH FIXED OR FREE TRANSITION, M_∞ = 0.765

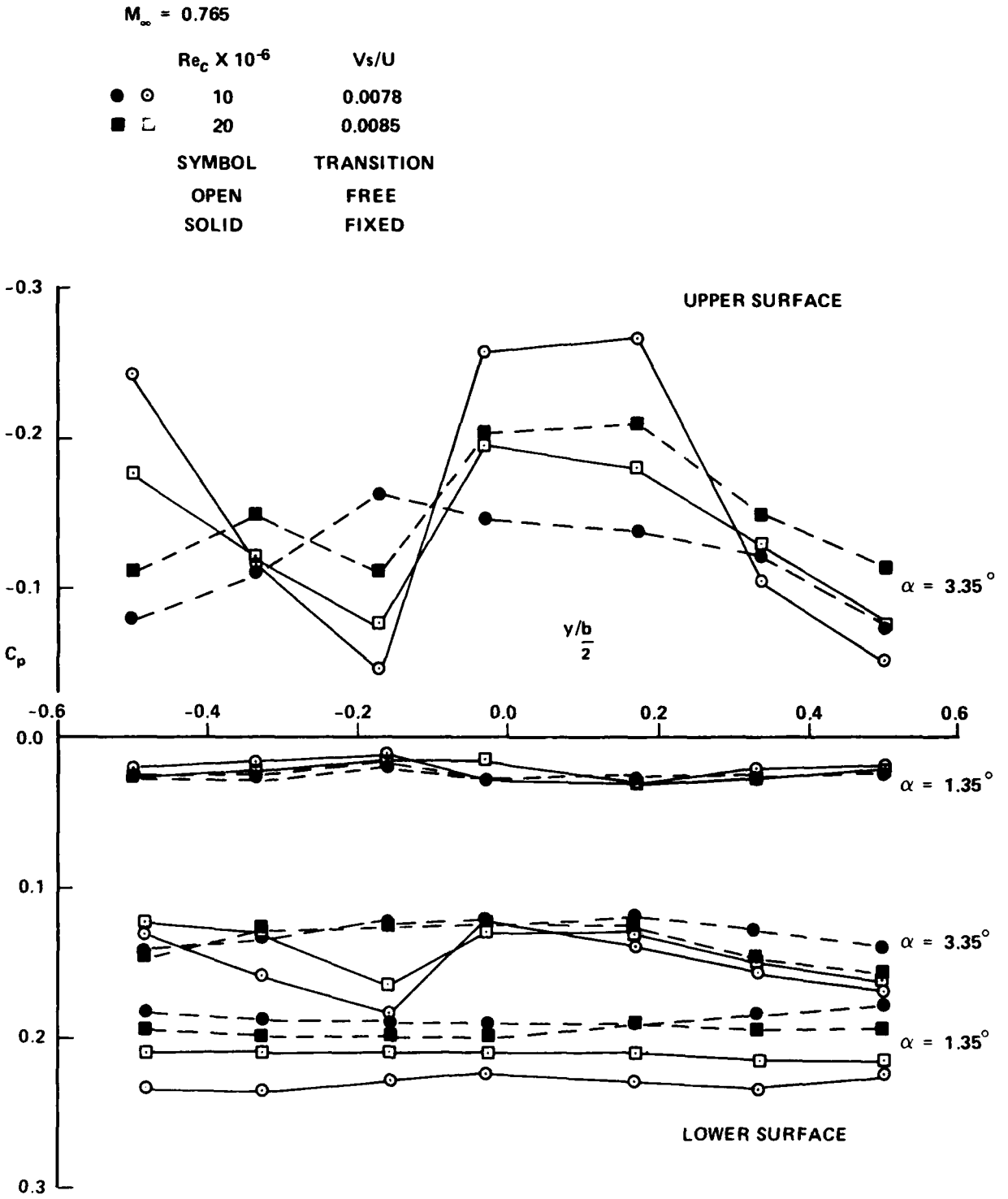

FIG. 5: SPANWISE PRESSURE DISTRIBUTIONS AT X/C = 0.9 FOR TWO ANGLES OF ATTACK AT VARIOUS REYNOLDS NUMBERS WITH FIXED OR FREE TRANSITION, M_∞ = 0.765

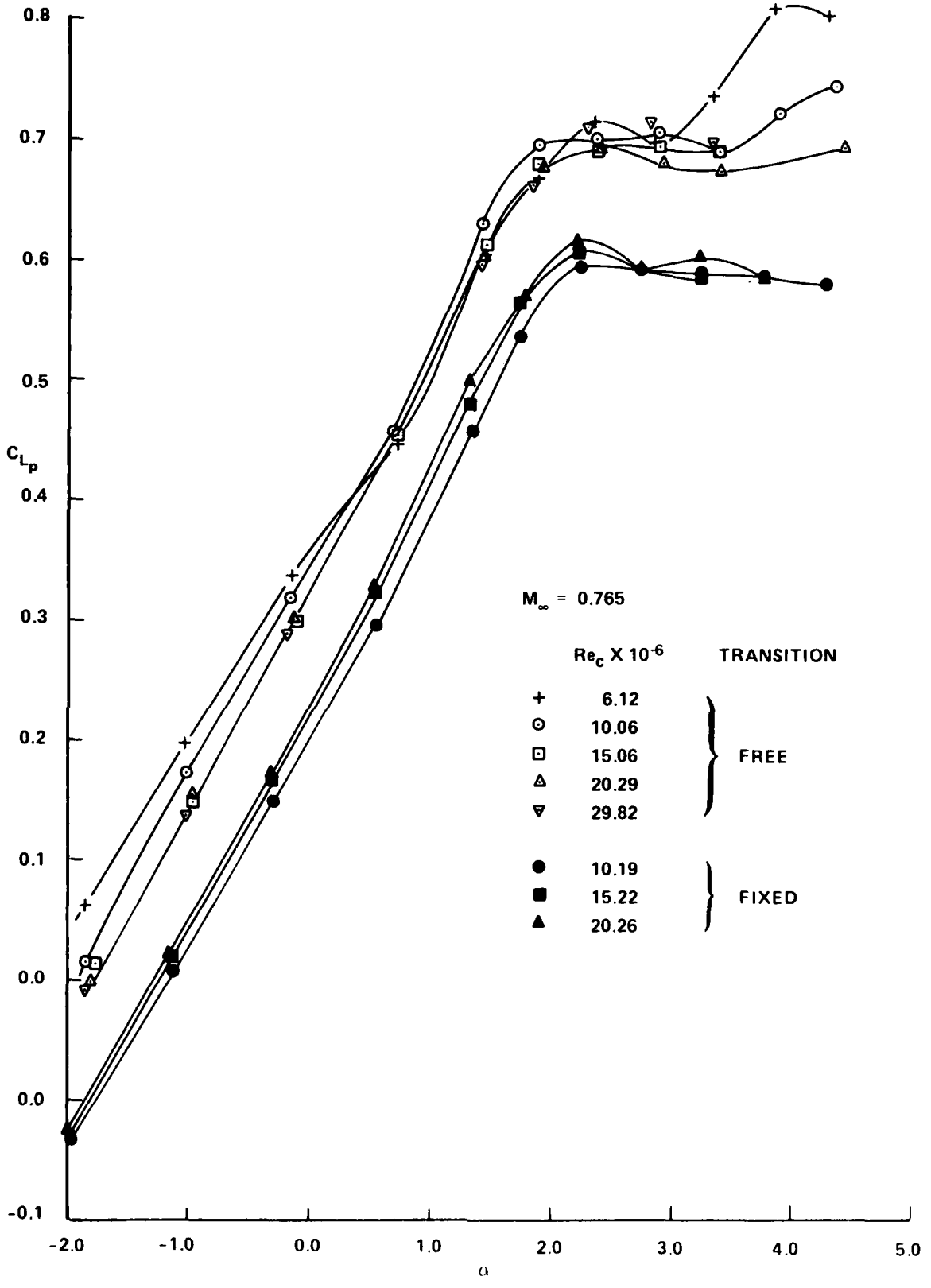

FIG. 6a: LIFT VERSUS ANGLE OF ATTACK AT VARIOUS REYNOLDS NUMBERS WITH FIXED OR FREE TRANSITION AT NOMINAL M_∞ = 0.765

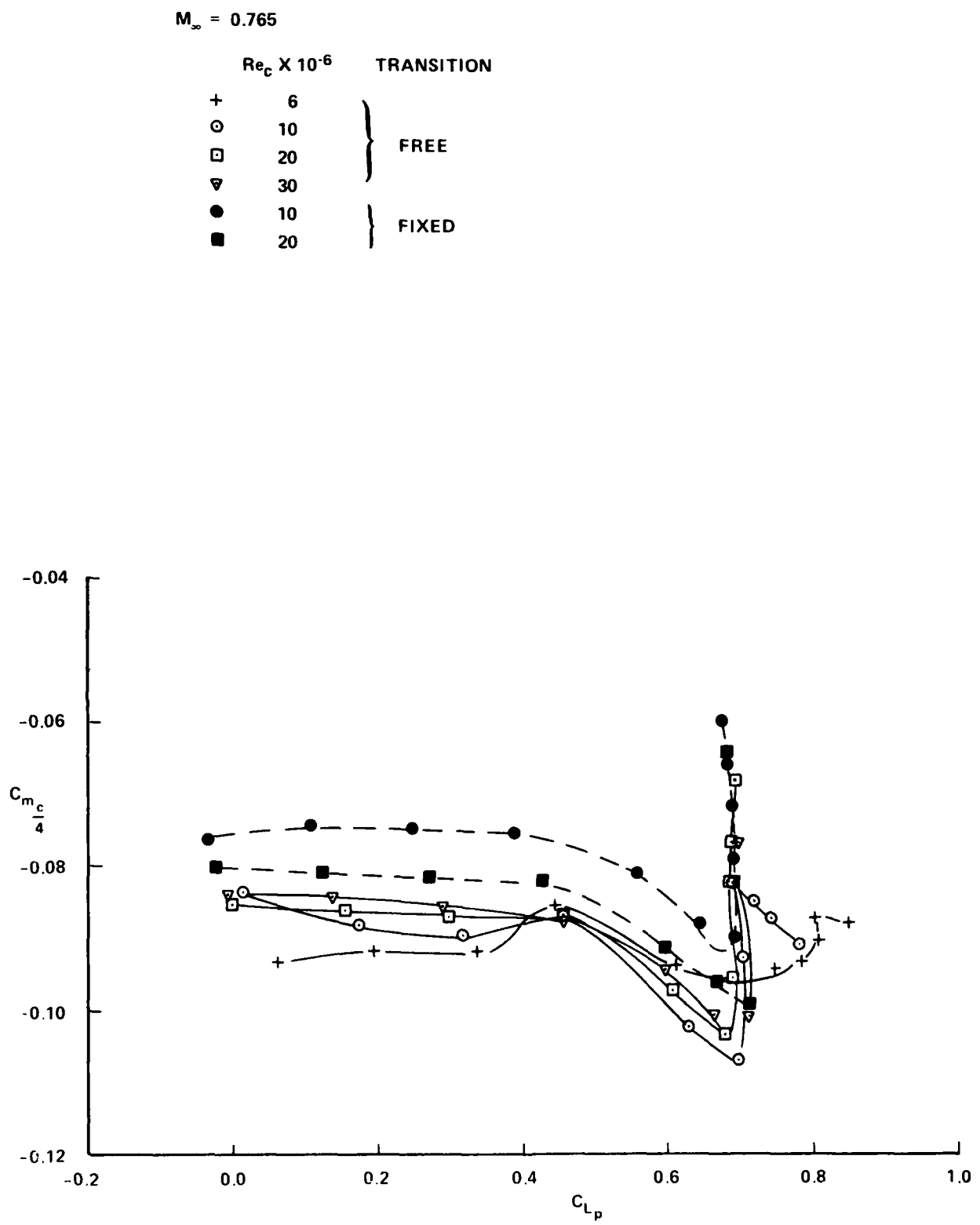

FIG. 6b: PITCHING MOMENT VERSUS LIFT AT VARIOUS REYNOLDS NUMBERS WITH FIXED OR FREE TRANSITION AT NOMINAL M_∞ = 0.765

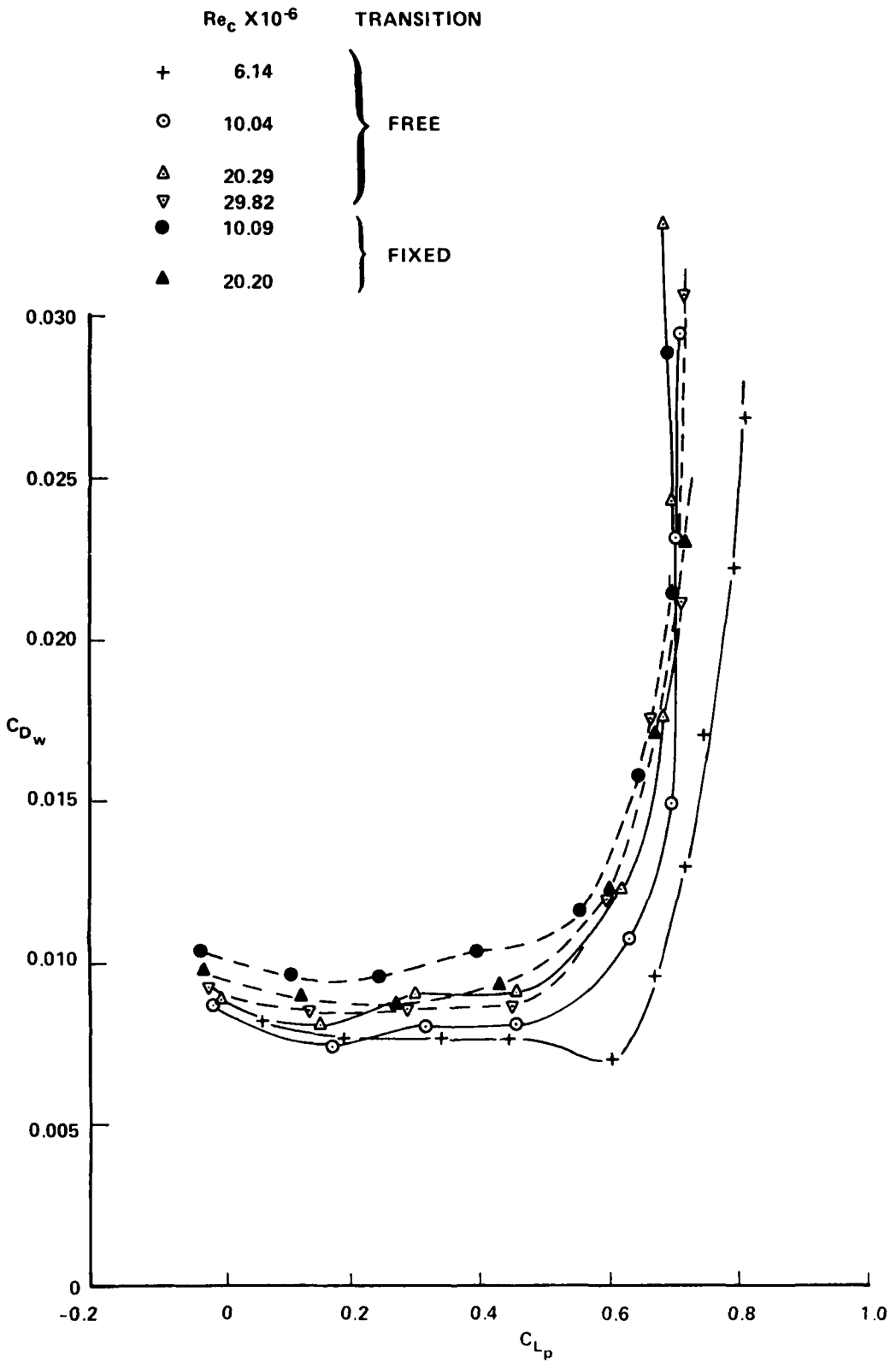

FIG. 6c: DRAG VERSUS LIFT AT VARIOUS REYNOLD NUMBERS WITH FIXED OR FREE TRANSITION AT NOMINAL M_∞ = 0.765

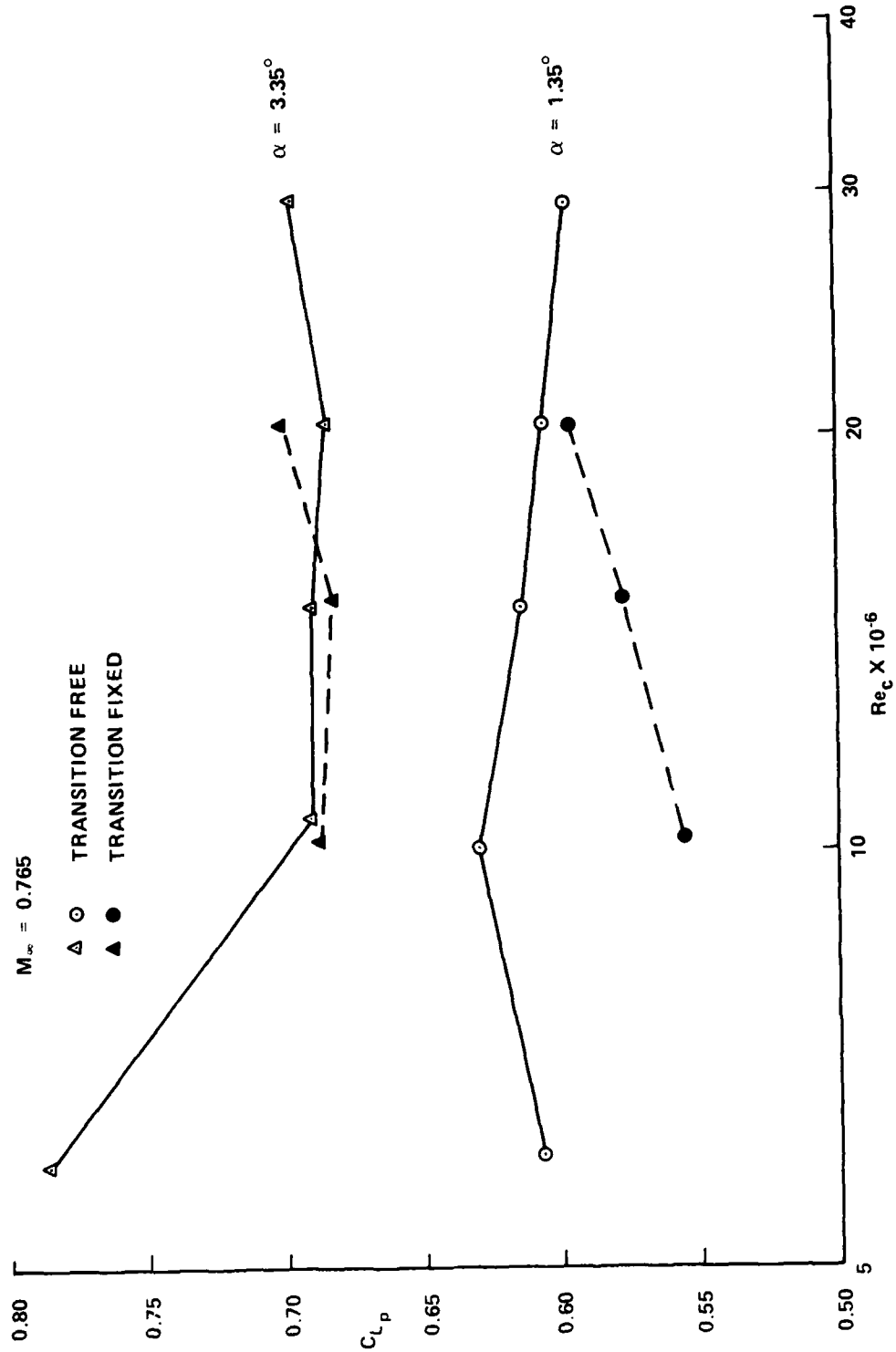

FIG. 6d: REYNOLDS NUMBER DEPENDENCE OF LIFT FOR TWO ANGLES OF ATTACK WITH FIXED OR FREE TRANSITION

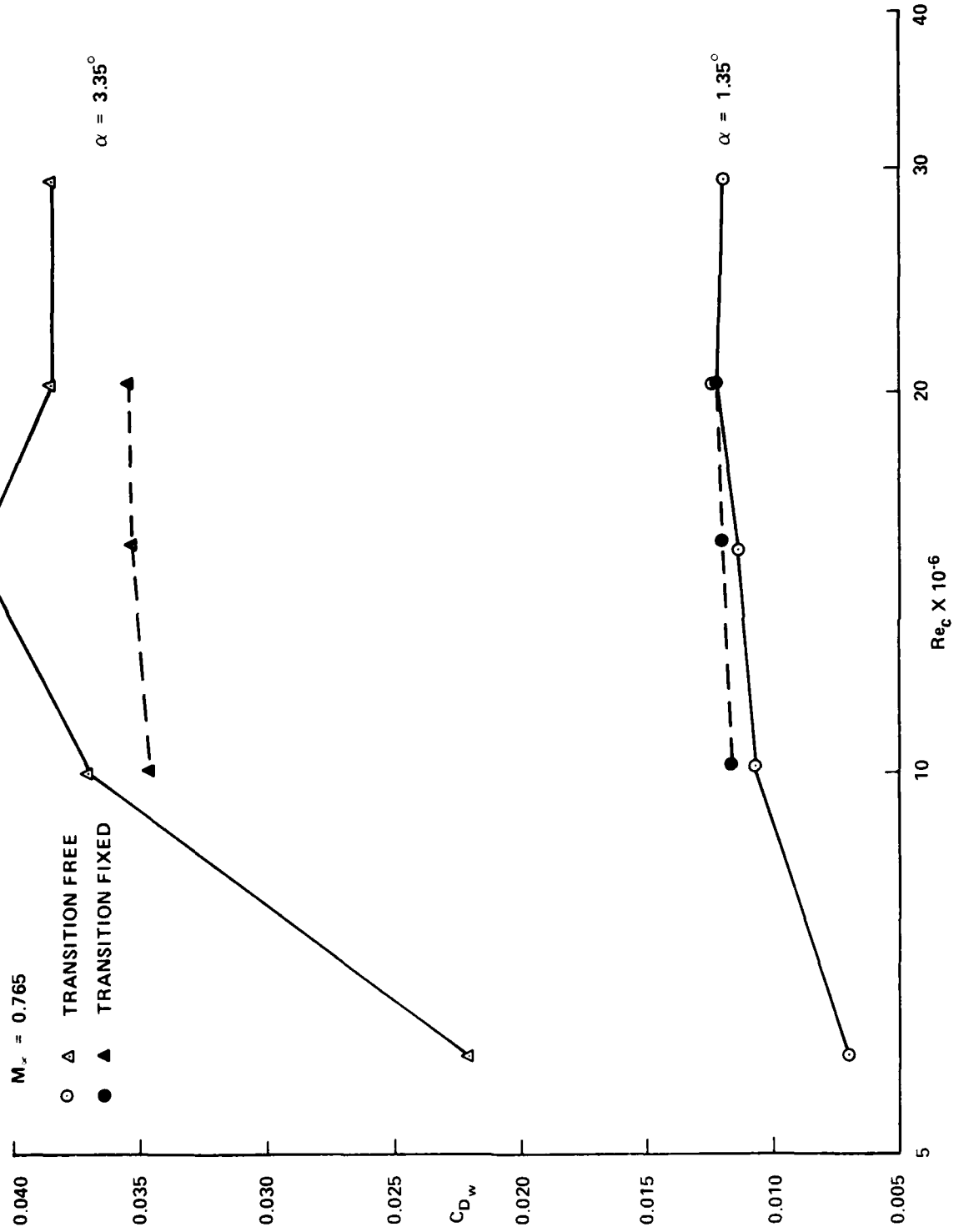

FIG. 6e: REYNOLDS NUMBER DEPENDENCE OF DRAG FOR TWO ANGLES OF ATTACK WITH FIXED OR FREE TRANSITION

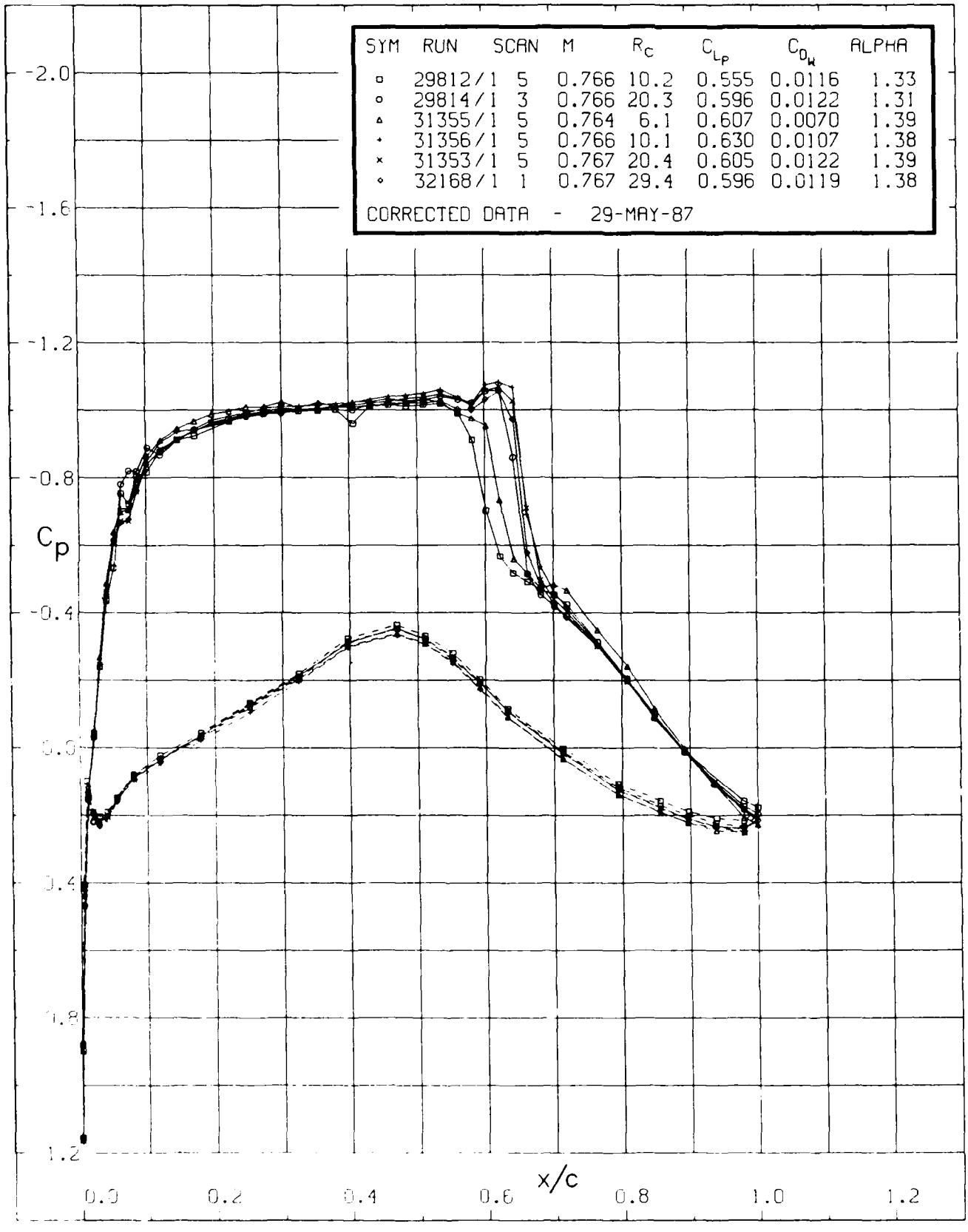

FIG. 7a: REYNOLDS NUMBER EFFECTS ON SURFACE PRESSURE DISTRIBUTIONS AT NOMINAL α = 1.35°, M_∞ = 0.765. THE FIRST TWO CASES ARE WITH TRANSITION FIXED, THE REST ARE TRANSITION FREE

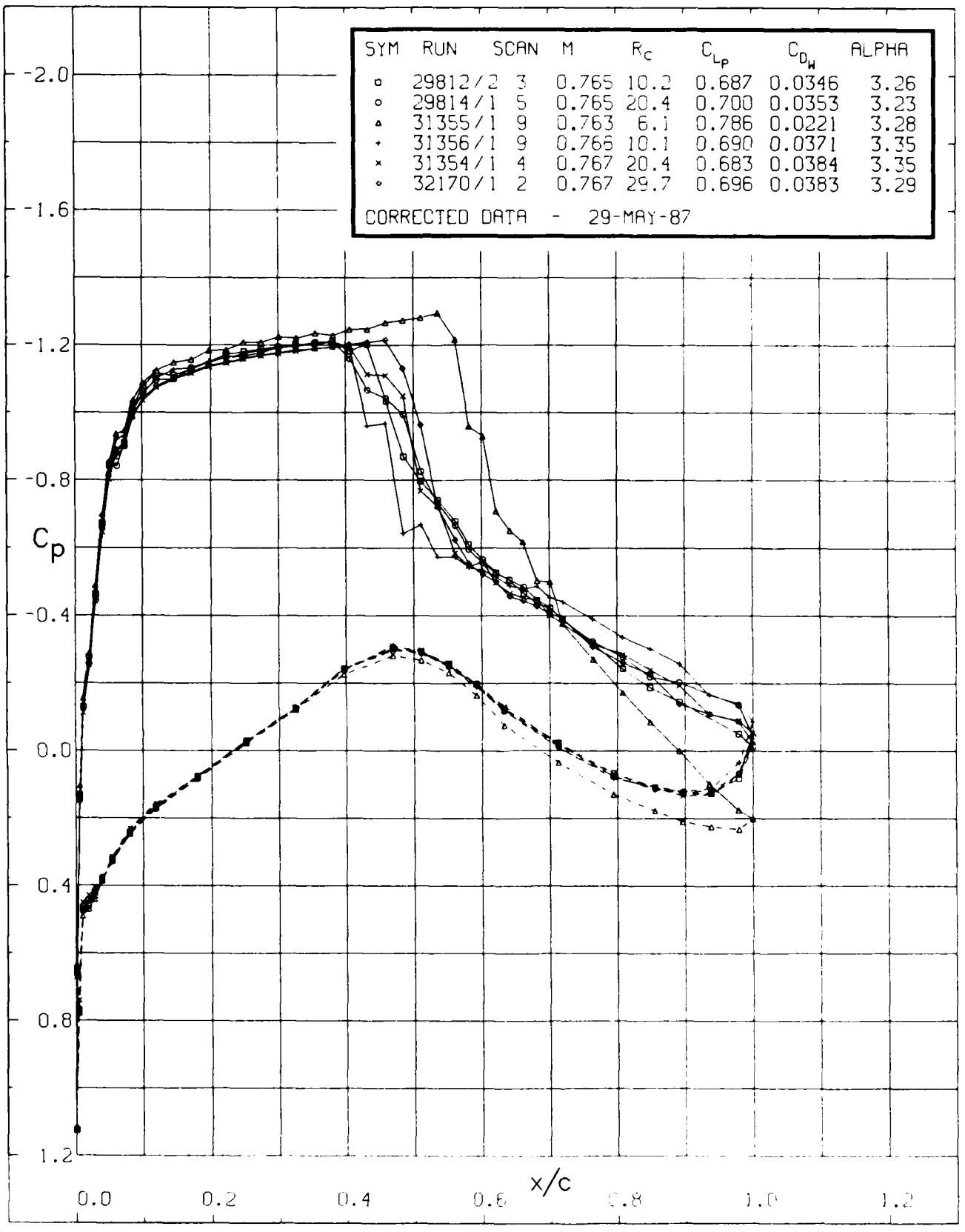

FIG. 7b: REYNOLDS NUMBER EFFECTS ON SURFACE PRESSURE DISTRIBUTIONS AT NOMINAL α = 3.35°, M_∞ = 0.765. THE FIRST TWO CASES ARE WITH TRANSITION FIXED, THE REST ARE TRANSITION FREE

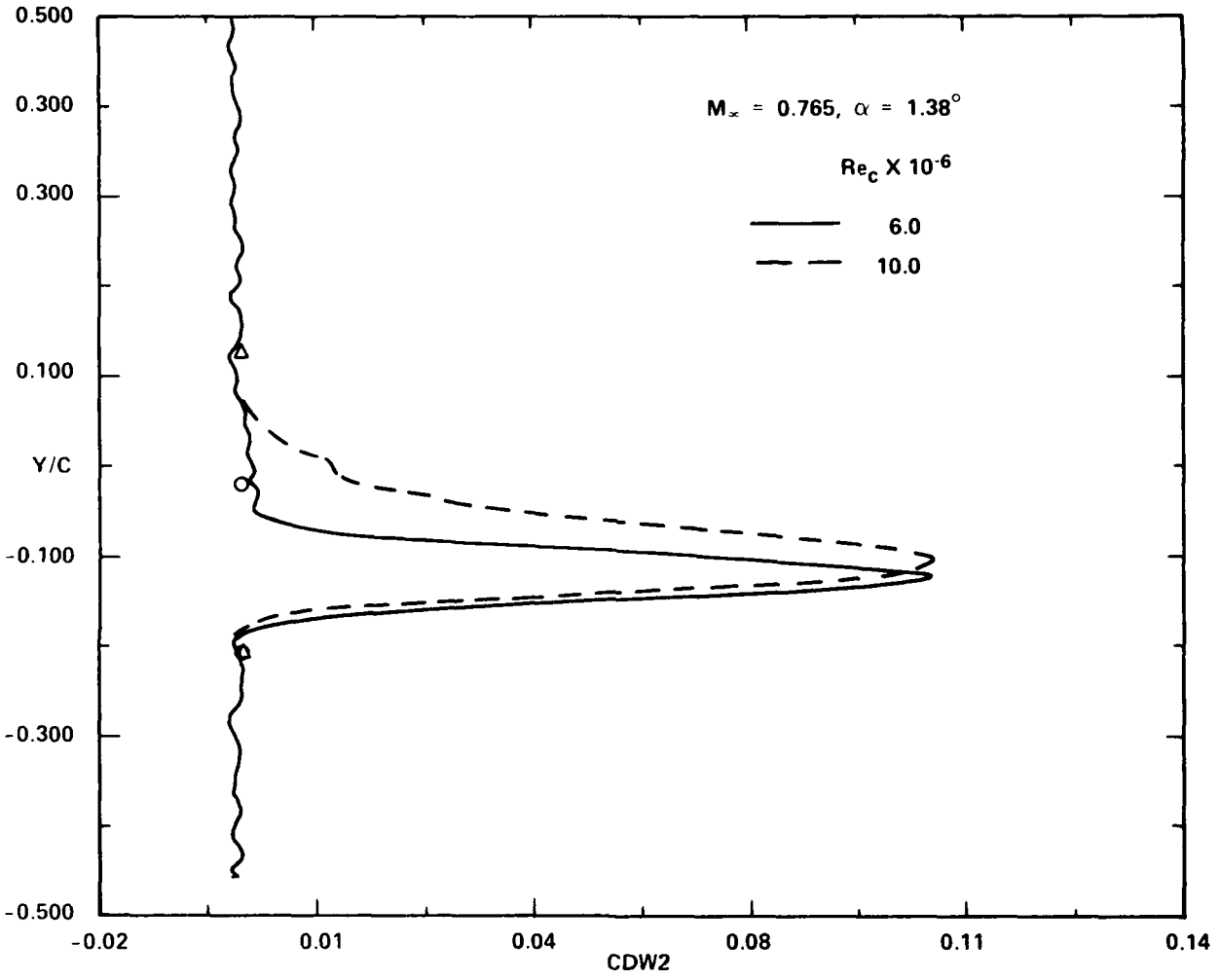

FIG. 8a: WAKE PROFILES SHOWING LAMINAR AND TURBULENT BOUNDARY LAYER SHOCK-WAVE INTERACTIONS RESPECTIVELY AT M_∞ = 0.765, α = 1.35°

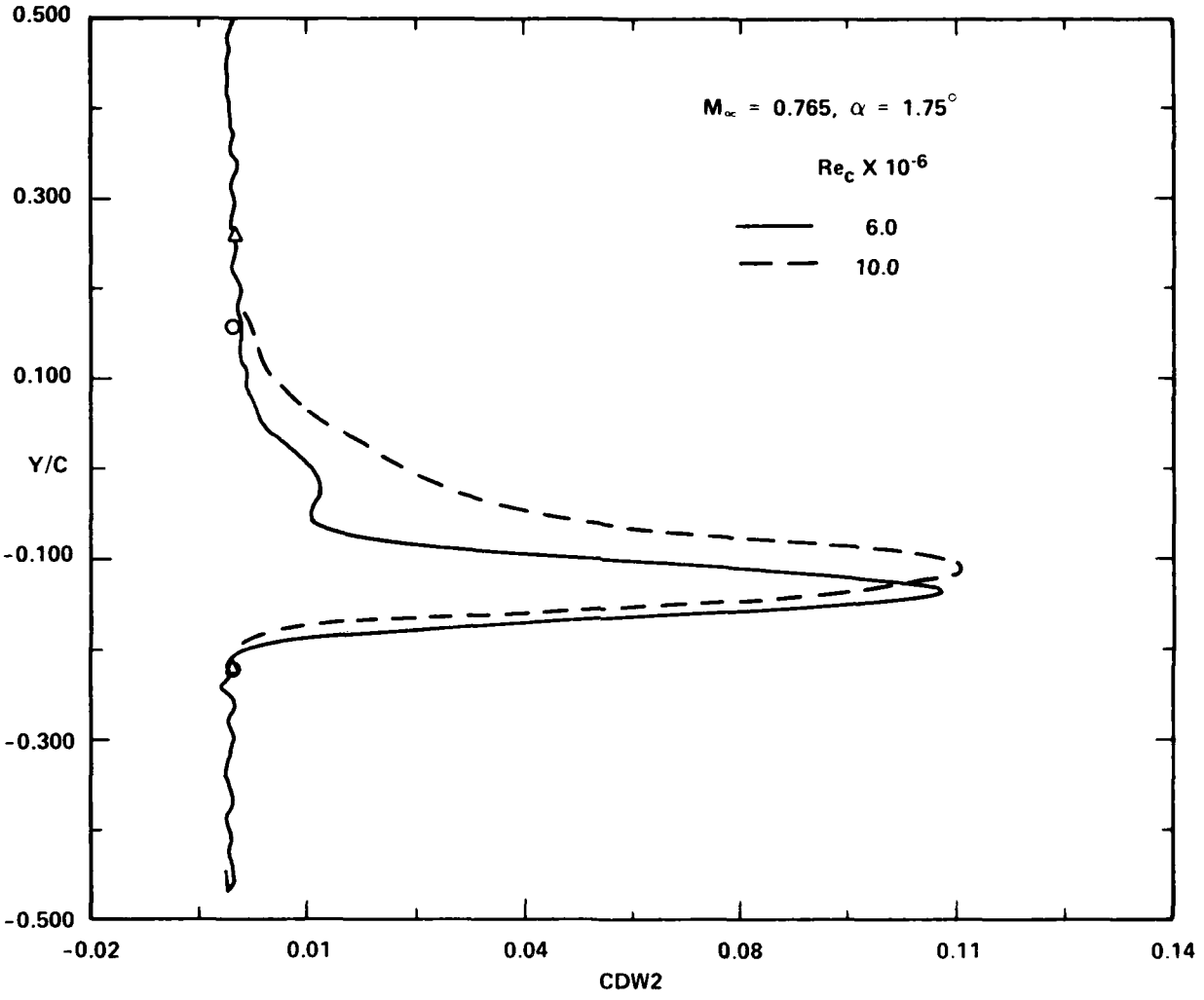

FIG. 8b: WAKE PROFILES SHOWING LAMINAR AND TURBULENT BOUNDARY LAYER SHOCK-WAVE INTERACTIONS RESPECTIVELY AT M_∞ = 0.765, α = 1.75°

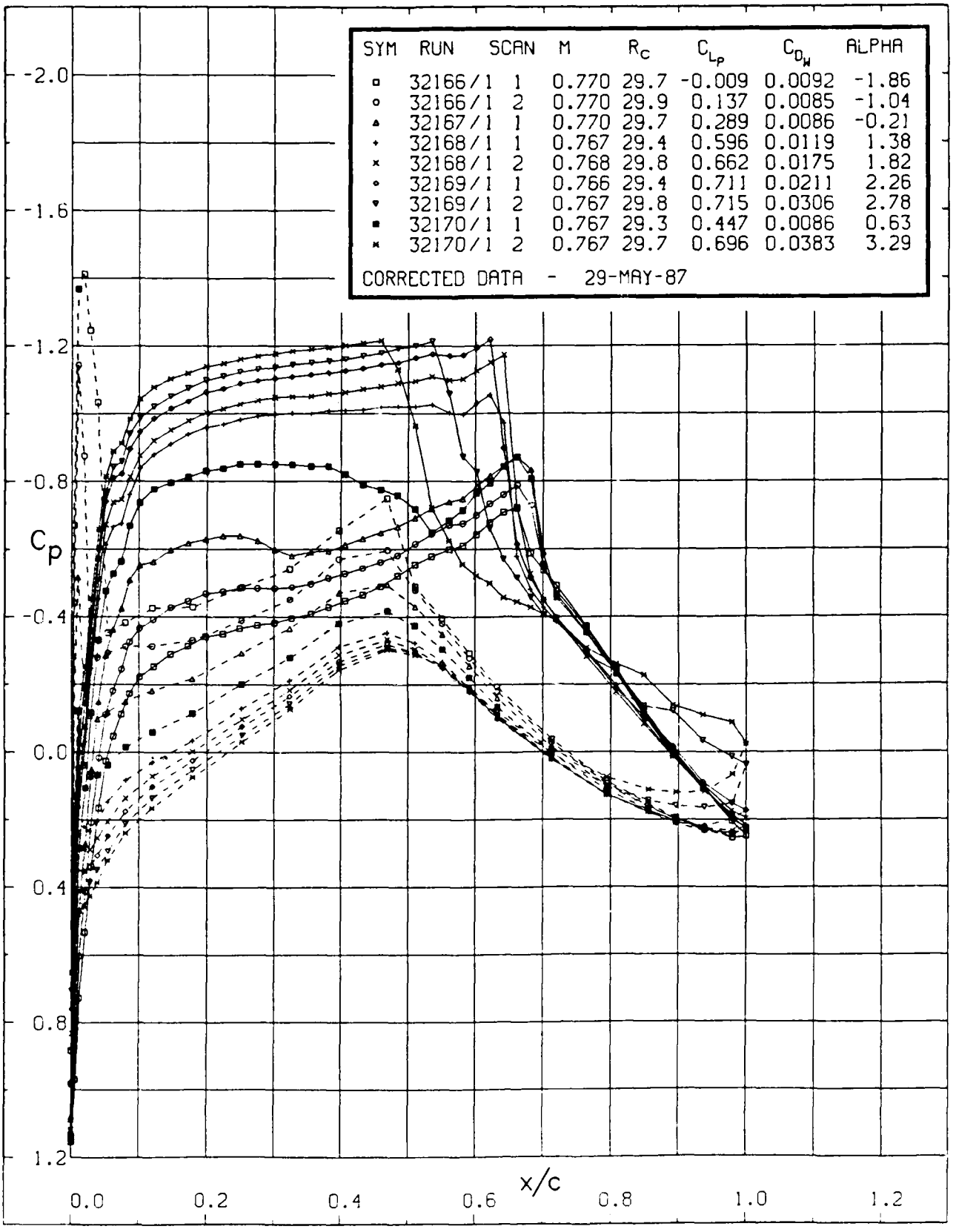

FIG. 9: SURFACE PRESSURE DISTRIBUTIONS AT DIFFERENT ANGLES OF ATTACK AT NOMINAL M_∞ = 0.765, Re_c = 30 X 10^6, TRANSITION FREE

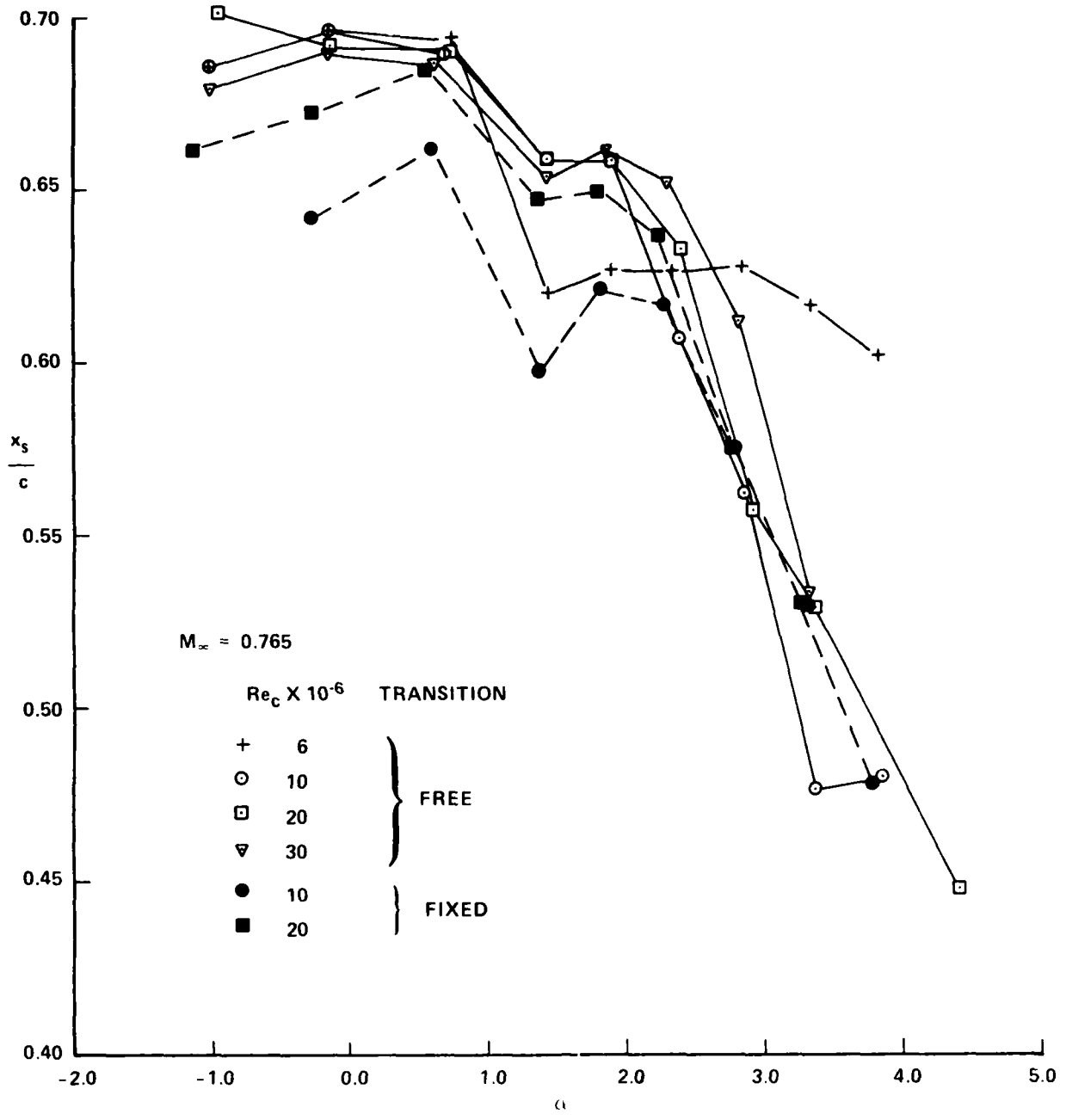

FIG. 10a: SHOCK LOCATION VERSUS ANGLE OF ATTACK AT VARIOUS REYNOLDS NUMBERS WITH FIXED OR FREE TRANSITION AT NOMINAL M_∞ = 0.765

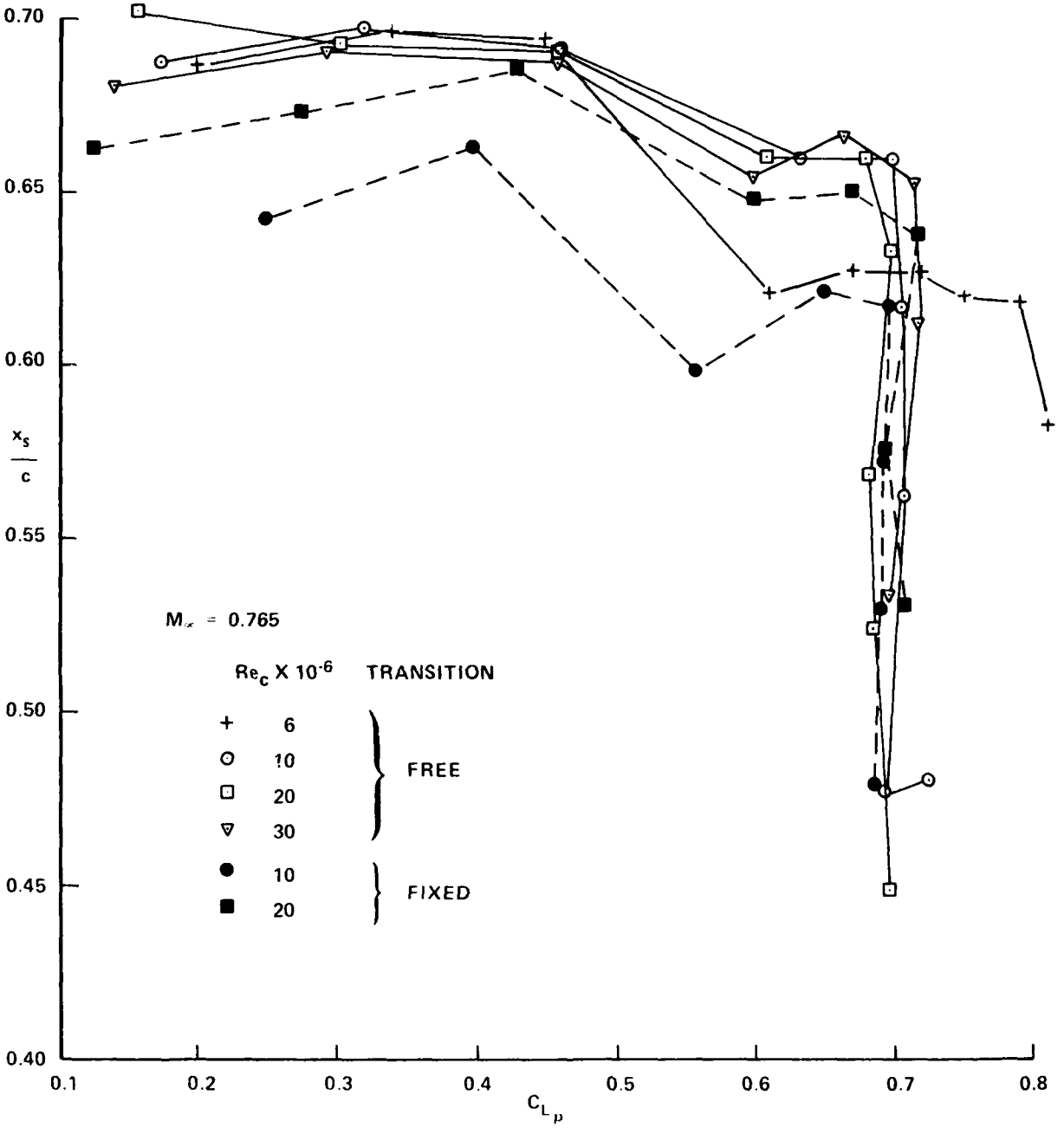

FIG. 10b: SHOCK LOCATION VERSUS LIFT AT VARIOUS REYNOLDS NUMBERS WITH FIXED OR FREE TRANSITION AT NOMINAL M_∞ = 0.765

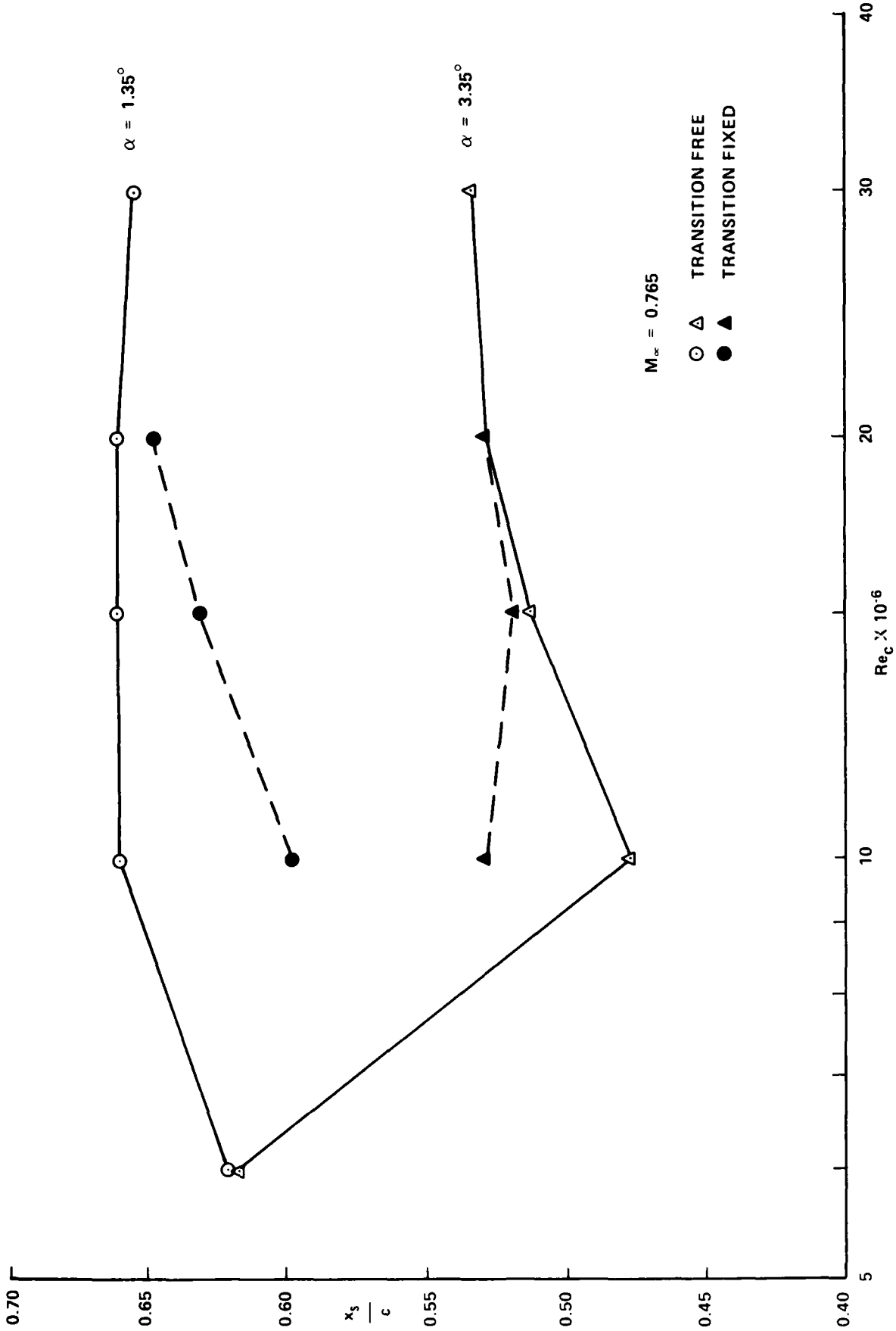

FIG. 10c: REYNOLDS NUMBER DEPENDENCE OF SHOCK LOCATION FOR TWO ANGLES OF ATTACK WITH FIXED OR FREE TRANSITION

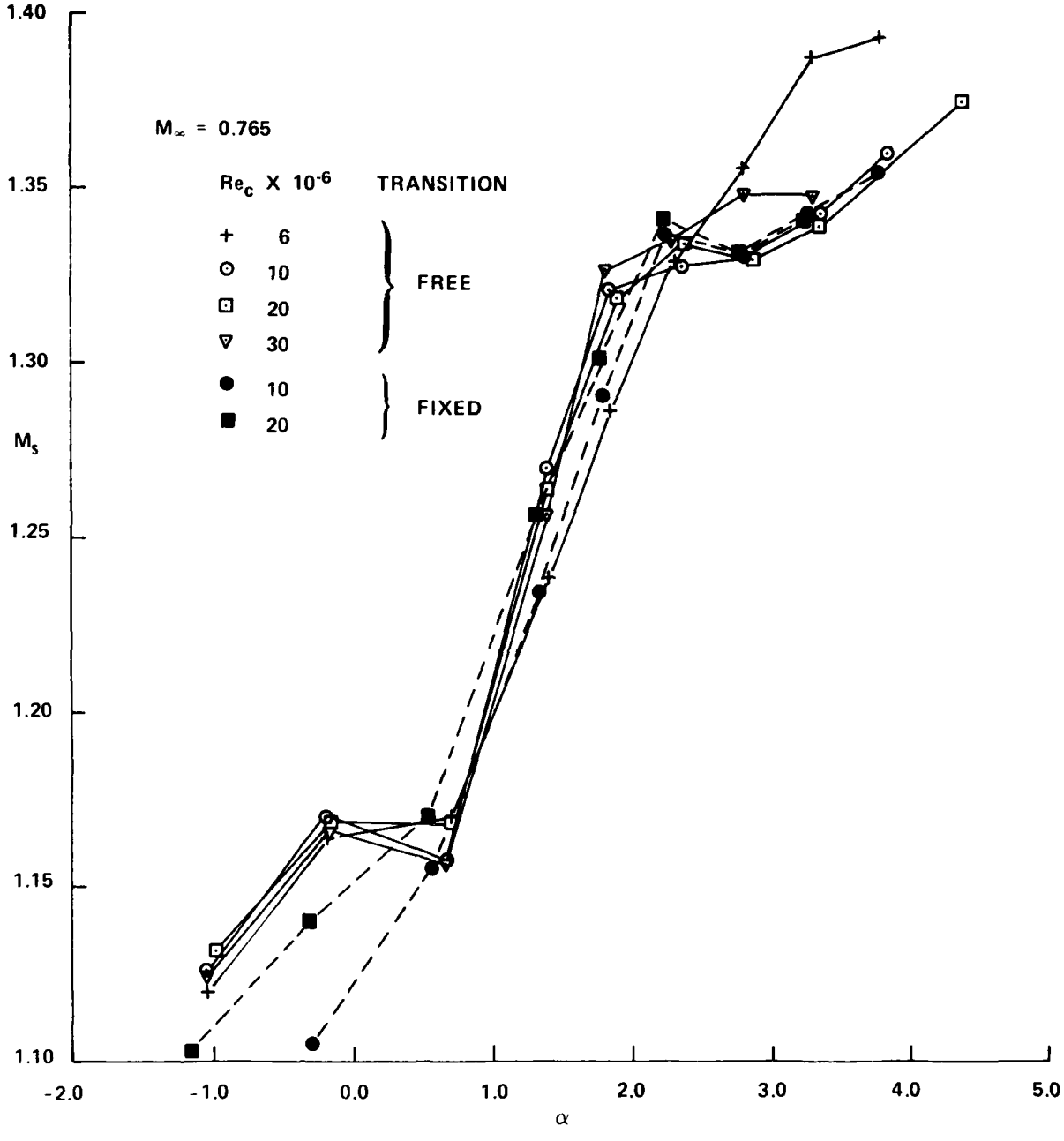

FIG. 11a: SHOCK MACH NUMBER VERSUS ANGLE OF ATTACK AT VARIOUS REYNOLDS NUMBERS WITH FIXED OR FREE TRANSITION AT NOMINAL M_∞ = 0.765

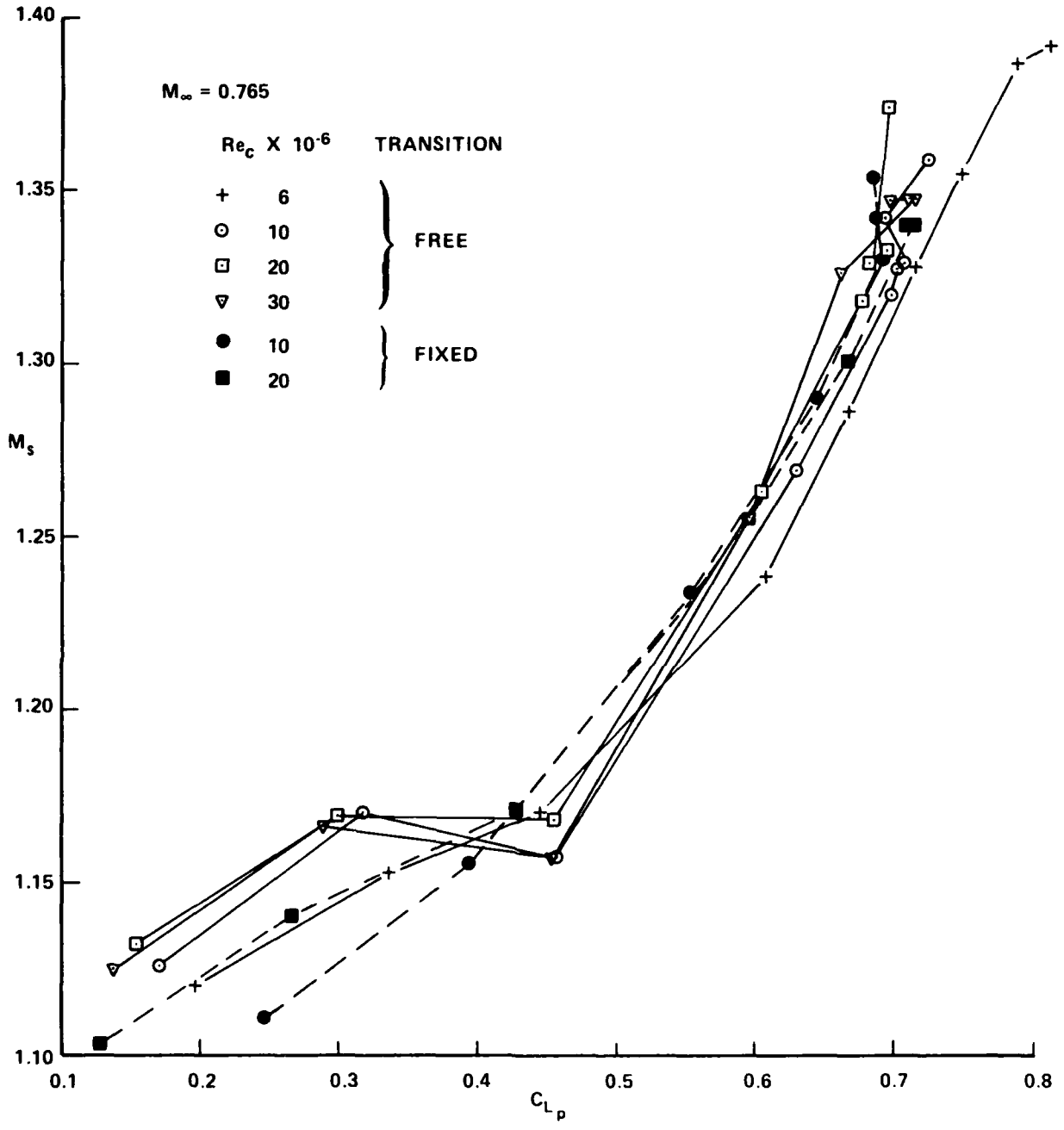

FIG. 11b: SHOCK MACH NUMBER VERSUS LIFT AT VARIOUS REYNOLDS NUMBERS WITH FIXED OR FREE TRANSITION AT NOMINAL M_∞ = 0.765

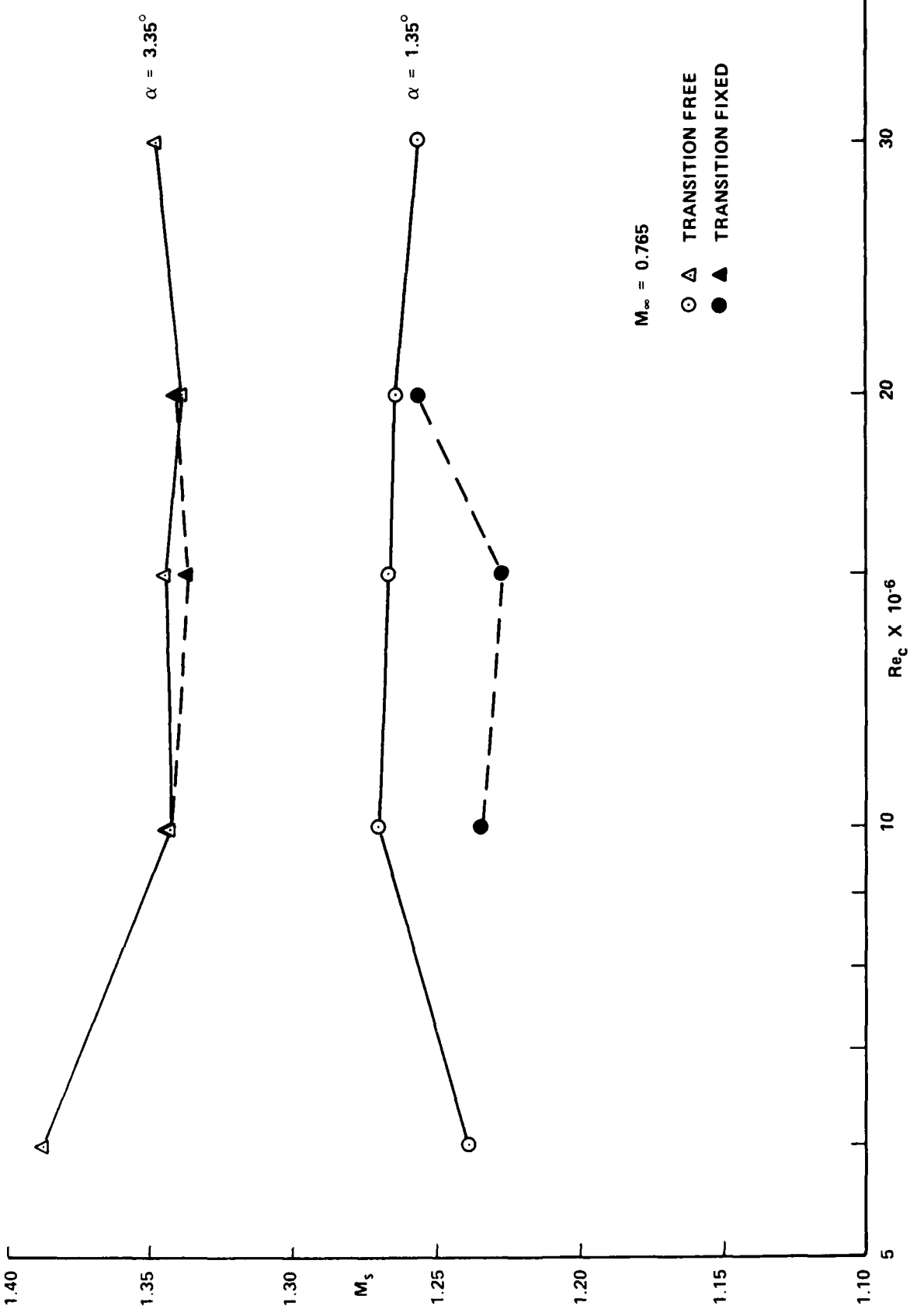

FIG. 11c: REYNOLDS NUMBER DEPENDENCE OF SHOCK MACH NUMBER FOR TWO ANGLES OF ATTACK WITH FIXED OR FREE TRANSITION

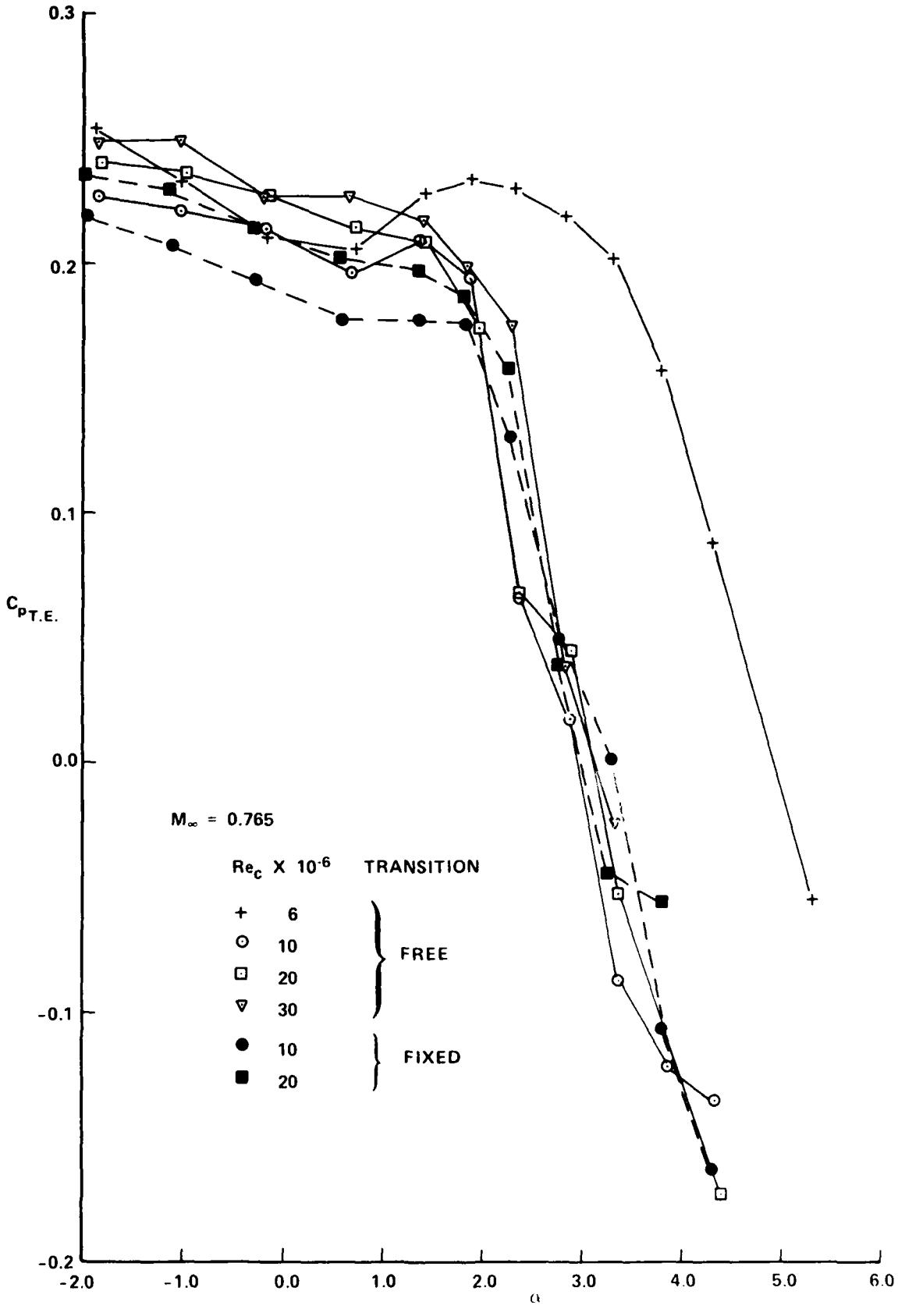

FIG. 12a: TRAILING EDGE PRESSURE VERSUS ANGLE OF ATTACK AT VARIOUS REYNOLDS NUMBERS WITH FIXED OR FREE TRANSITION AT NOMINAL M_∞ = 0.765

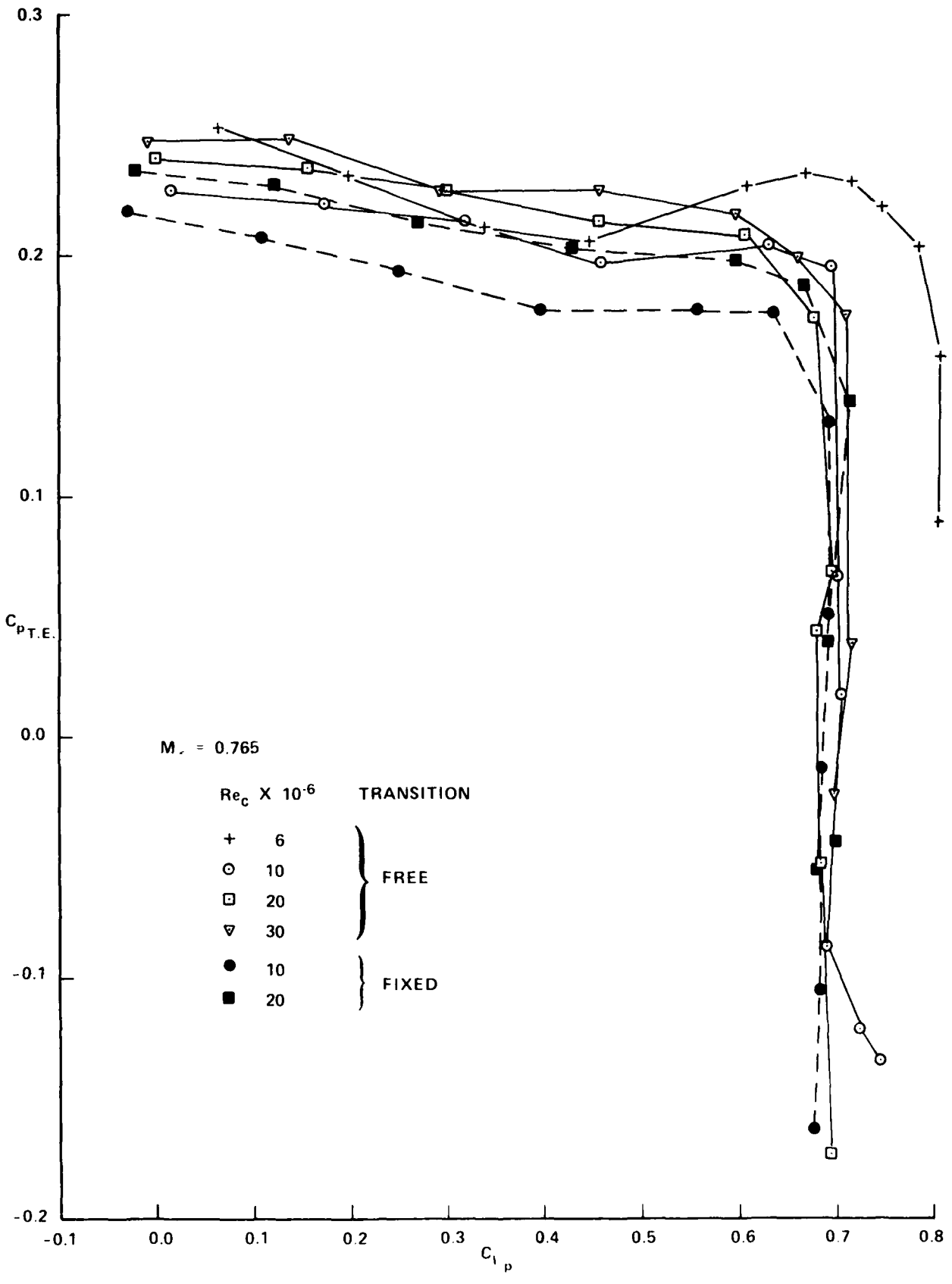

FIG. 12b: TRAILING EDGE PRESSURE VERSUS LIFT AT VARIOUS REYNOLDS NUMBERS WITH FIXED OR FREE TRANSITION AT NOMINAL M_∞ = 0.765

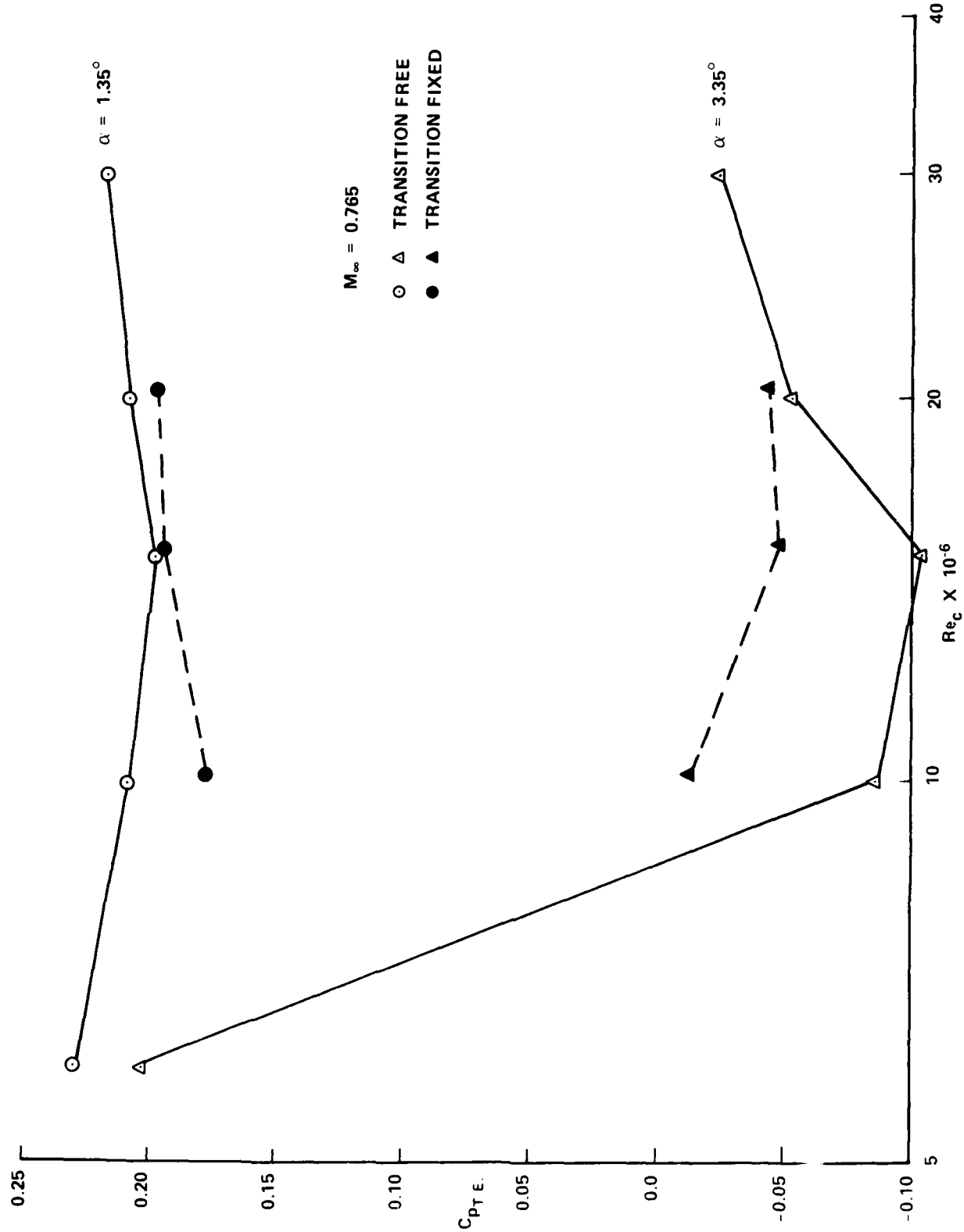

FIG. 12c: REYNOLDS NUMBER DEPENDENCY OF TRAILING EDGE PRESSURE FOR TWO ANGLES OF ATTACK WITH FIXED AND FREE TRANSITION

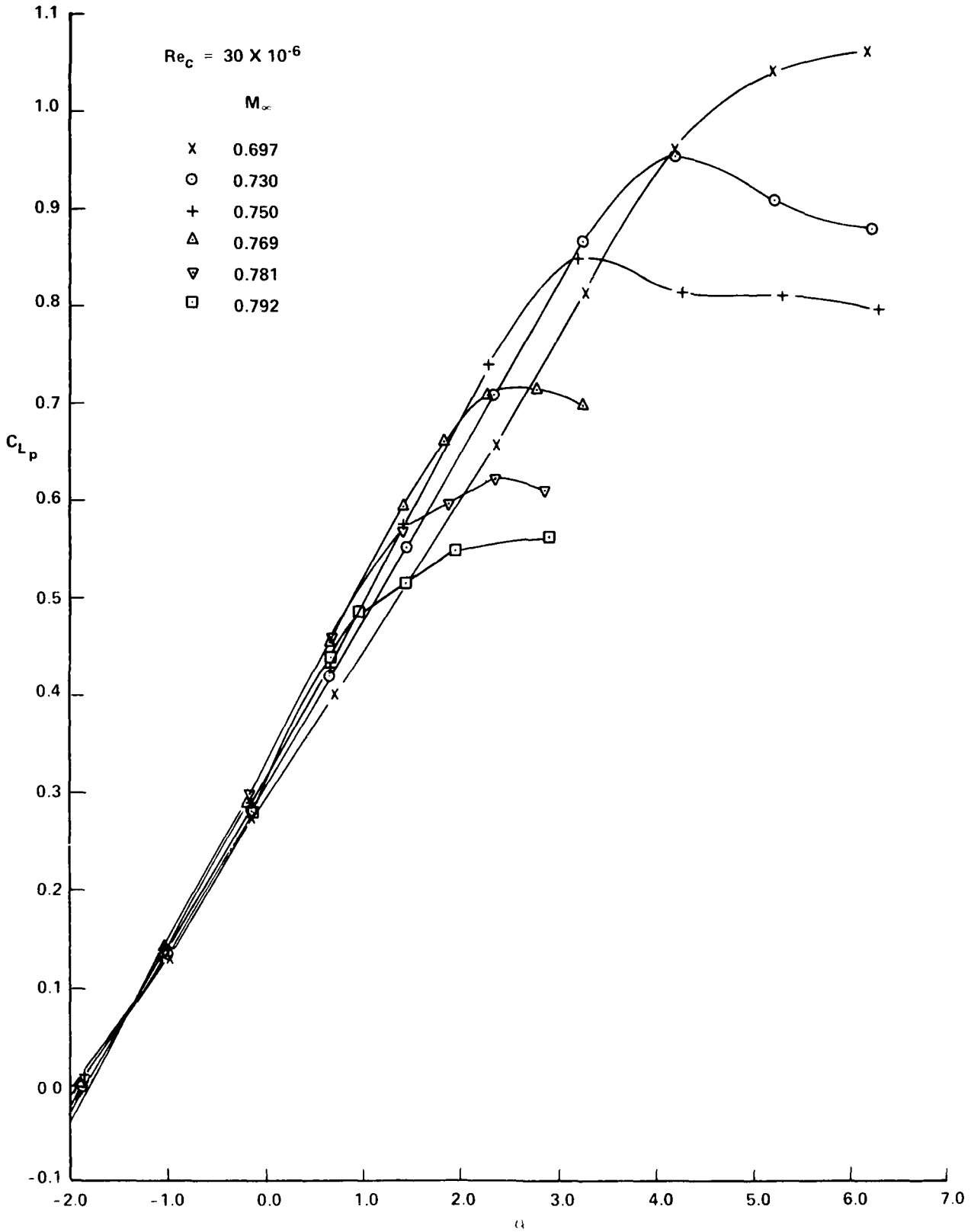

FIG. 13a: LIFT VERSUS ANGLE OF ATTACK AT VARIOUS MACH NUMBERS AT NOMINAL Re_c = 30 X 10^6 WITH FREE TRANSITION

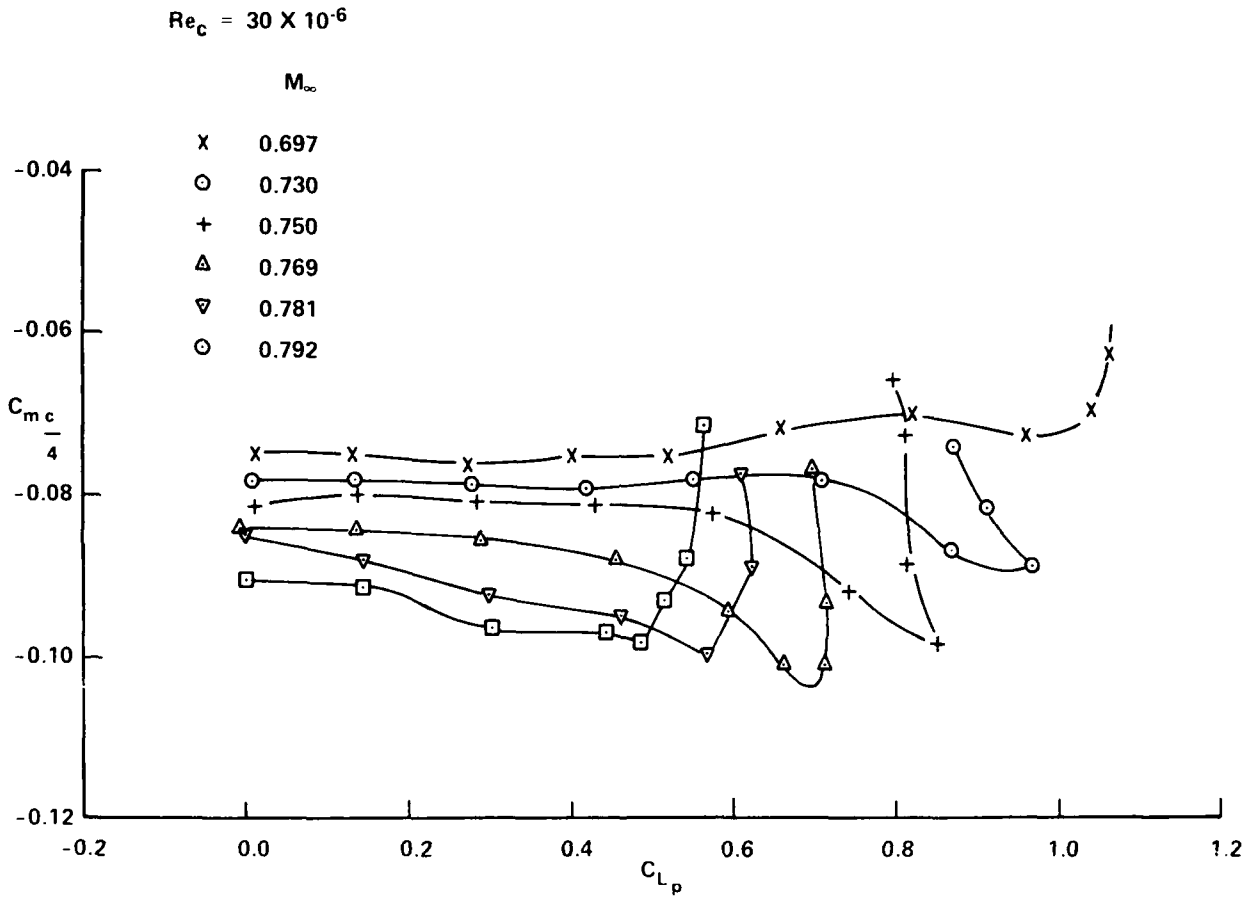

FIG. 13b: PITCHING MOMENT VERSUS LIFT AT VARIOUS MACH NUMBERS AT NOMINAL Re_c = 30 X 10^6 WITH FREE TRANSITION

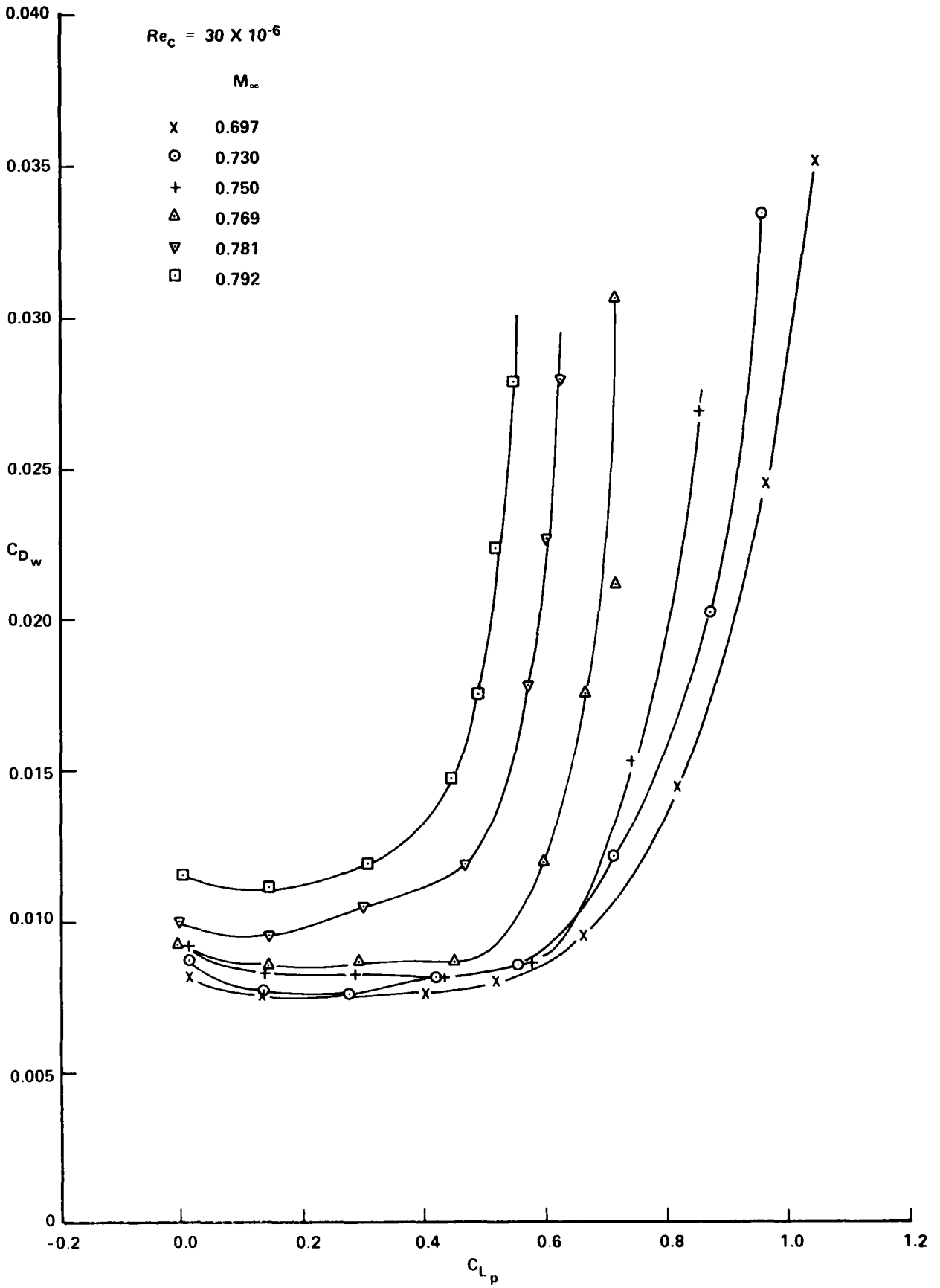

FIG. 13c: DRAG VERSUS LIFT AT VARIOUS MACH NUMBERS AT NOMINAL Re_c = 30 X 10^6 WITH FREE TRANSITION

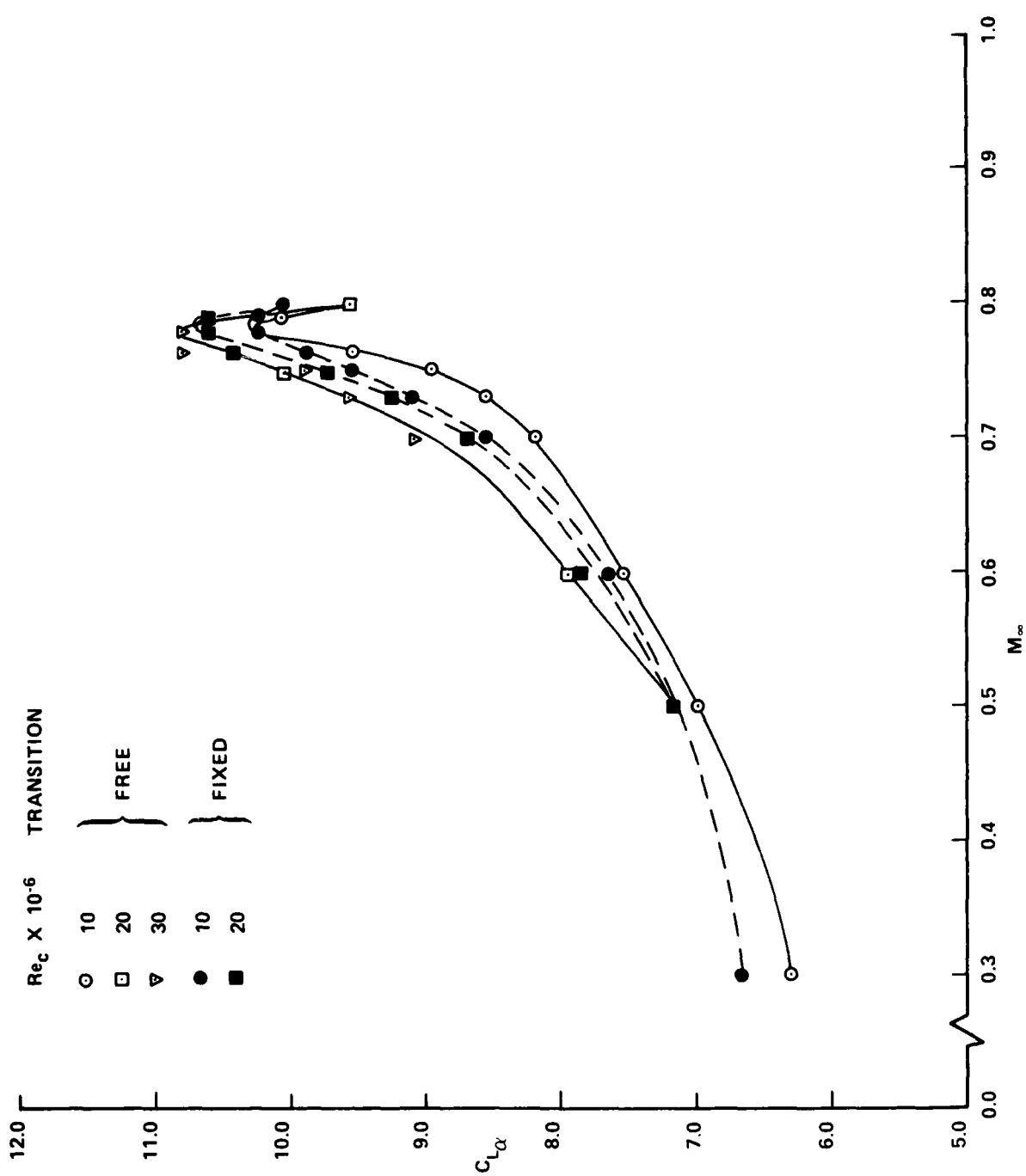

FIG. 14: LIFT CURVE SLOP AT ZERO LIFT VERSUS MACH NUMBER AT VARIOUS REYNOLDS NUMBERS WITH FIXED OR FREE TRANSITION

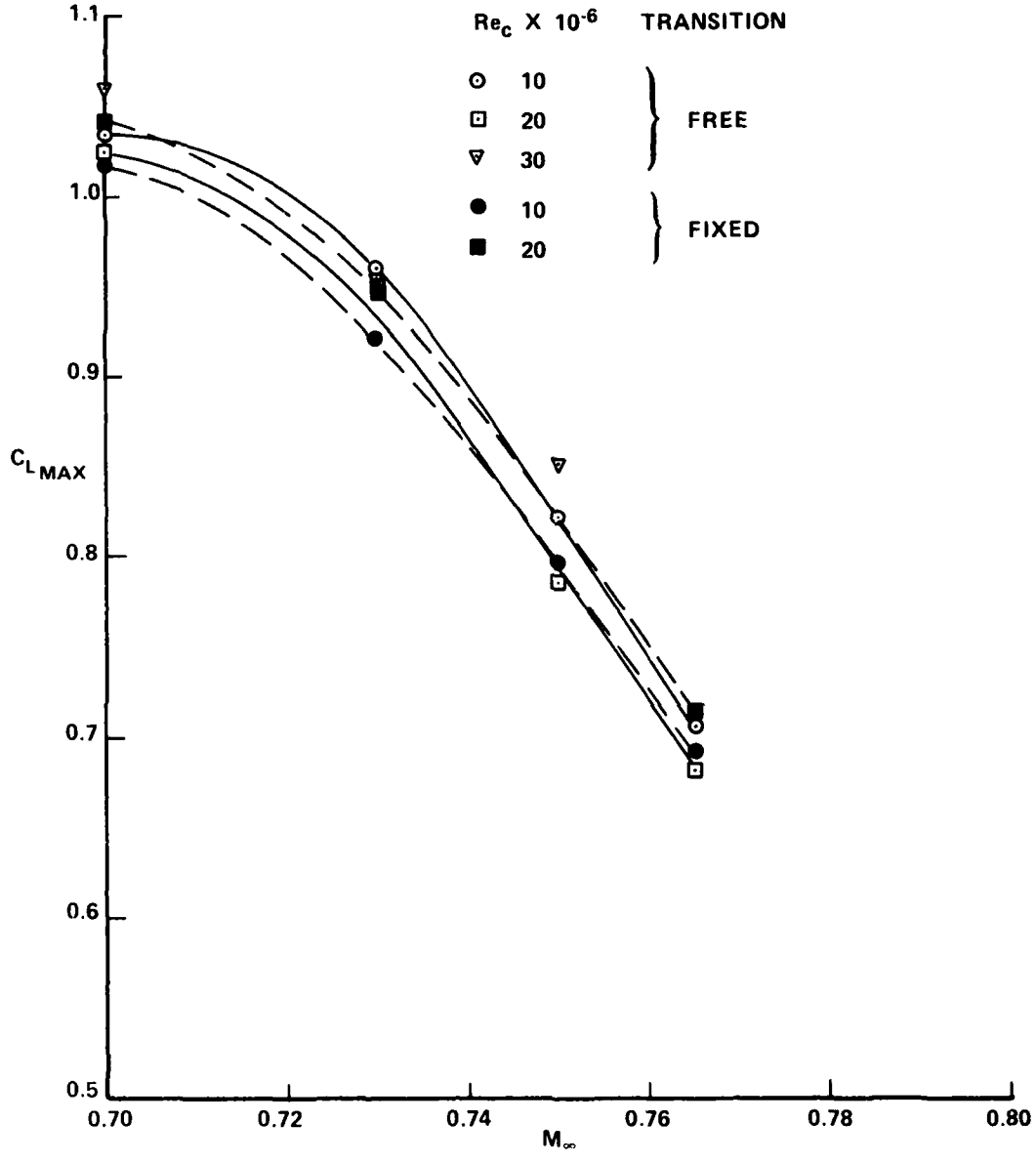

FIG. 15a: MAXIMUM LIFT VERSUS MACH NUMBER AT VARIOUS REYNOLDS NUMBERS WITH FIXED OR FREE TRANSITION

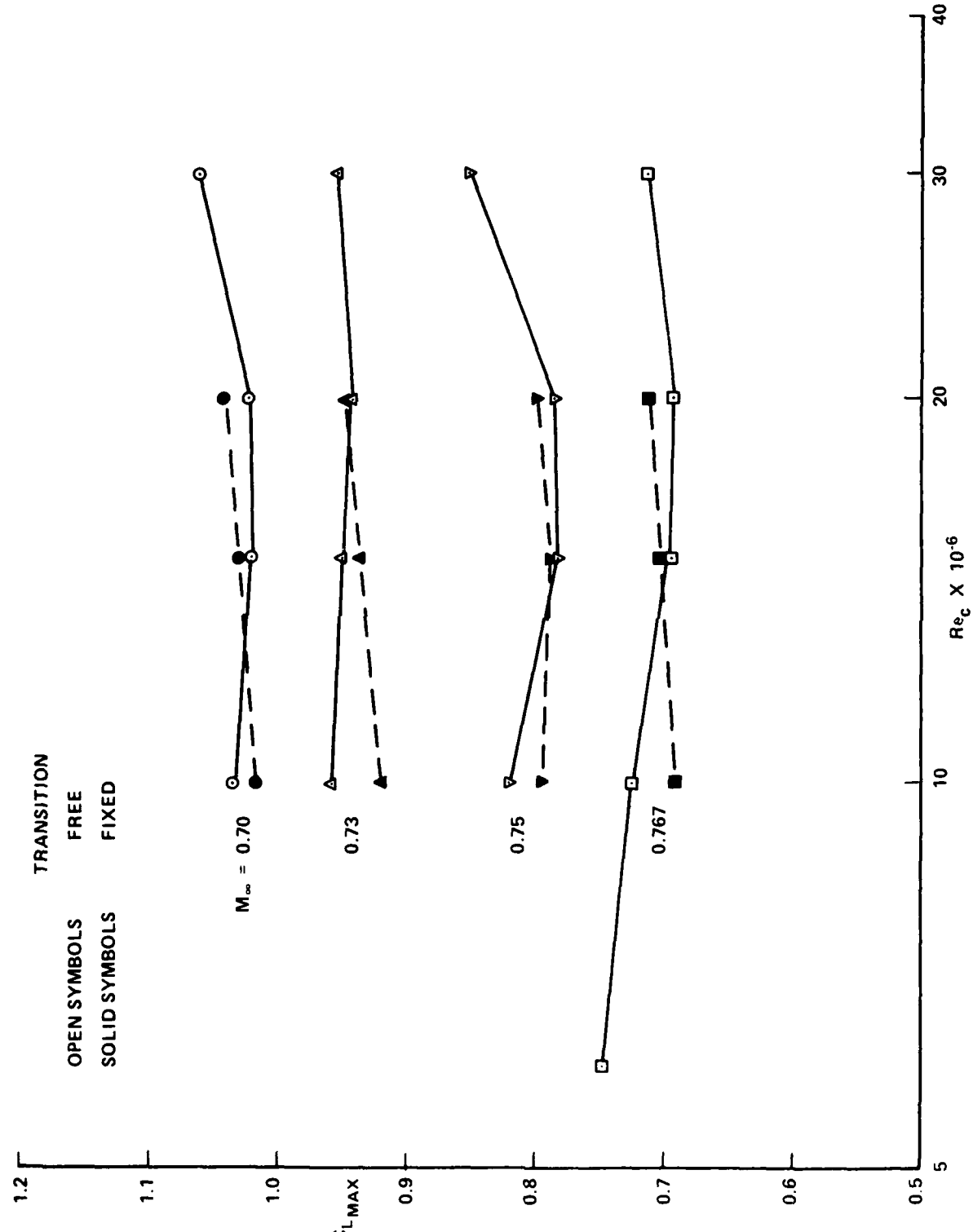

FIG. 15b: REYNOLDS NUMBER DEPENDENCE OF MAXIMUM LIFT AT VARIOUS MACH NUMBERS WITH FIXED OR FREE TRANSITION

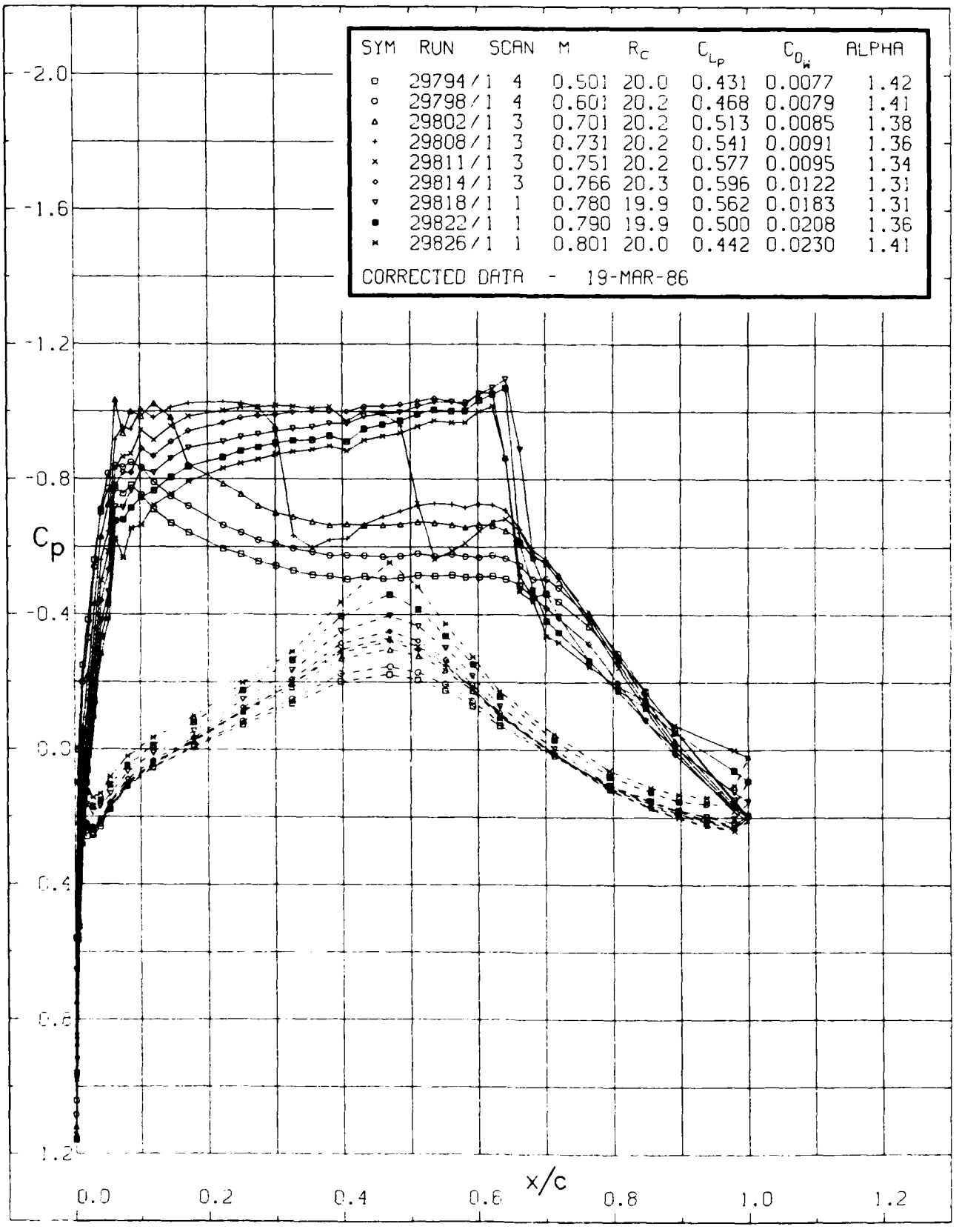

FIG. 16a: MACH NUMBER EFFECTS ON SURFACE PRESSURE DISTRIBUTIONS AT NOMINAL α = 1.35°, Re_c = 20 X 10^6 WITH FIXED TRANSITION

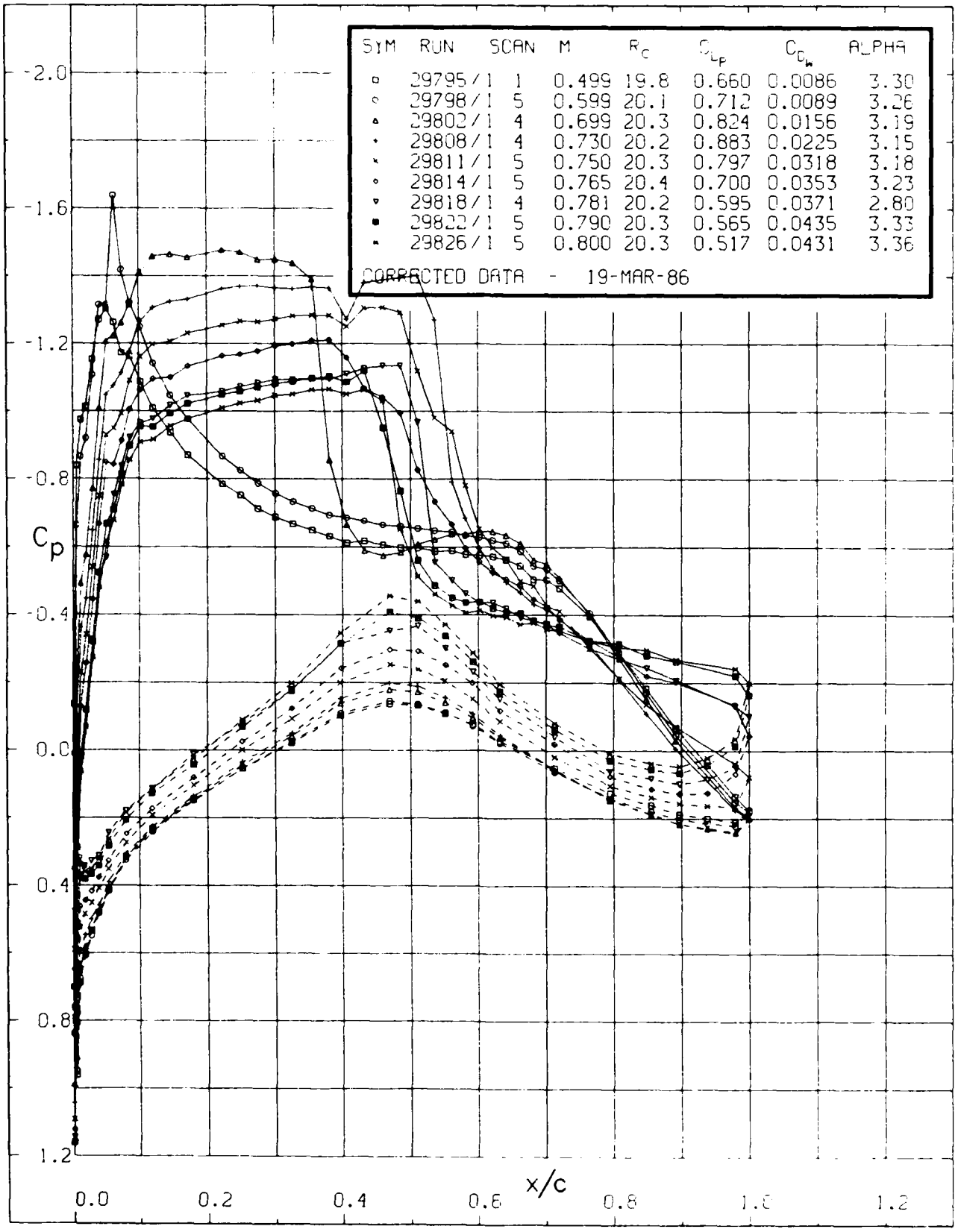

FIG. 16b: MACH NUMBER EFFECTS ON SURFACE PRESSURE DISTRIBUTIONS AT NOMINAL α = 3.35°, Re_c = 20 X 10^6 WITH FIXED TRANSITION

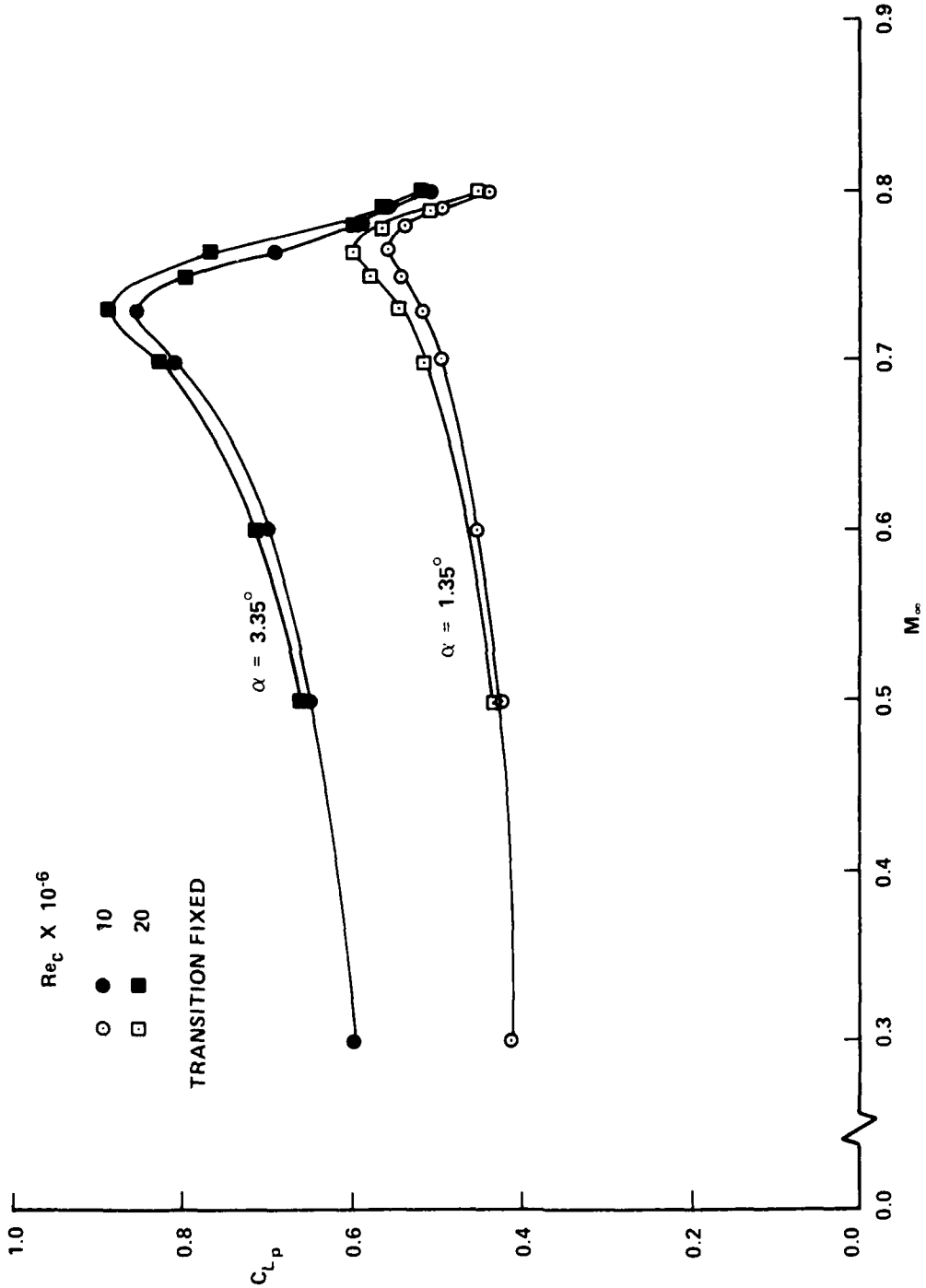

FIG. 17a: MACH NUMBER AND REYNOLDS NUMBER DEPENDENCE OF LIFT AT TWO ANGLES OF ATTACK WITH FIXED TRANSITION

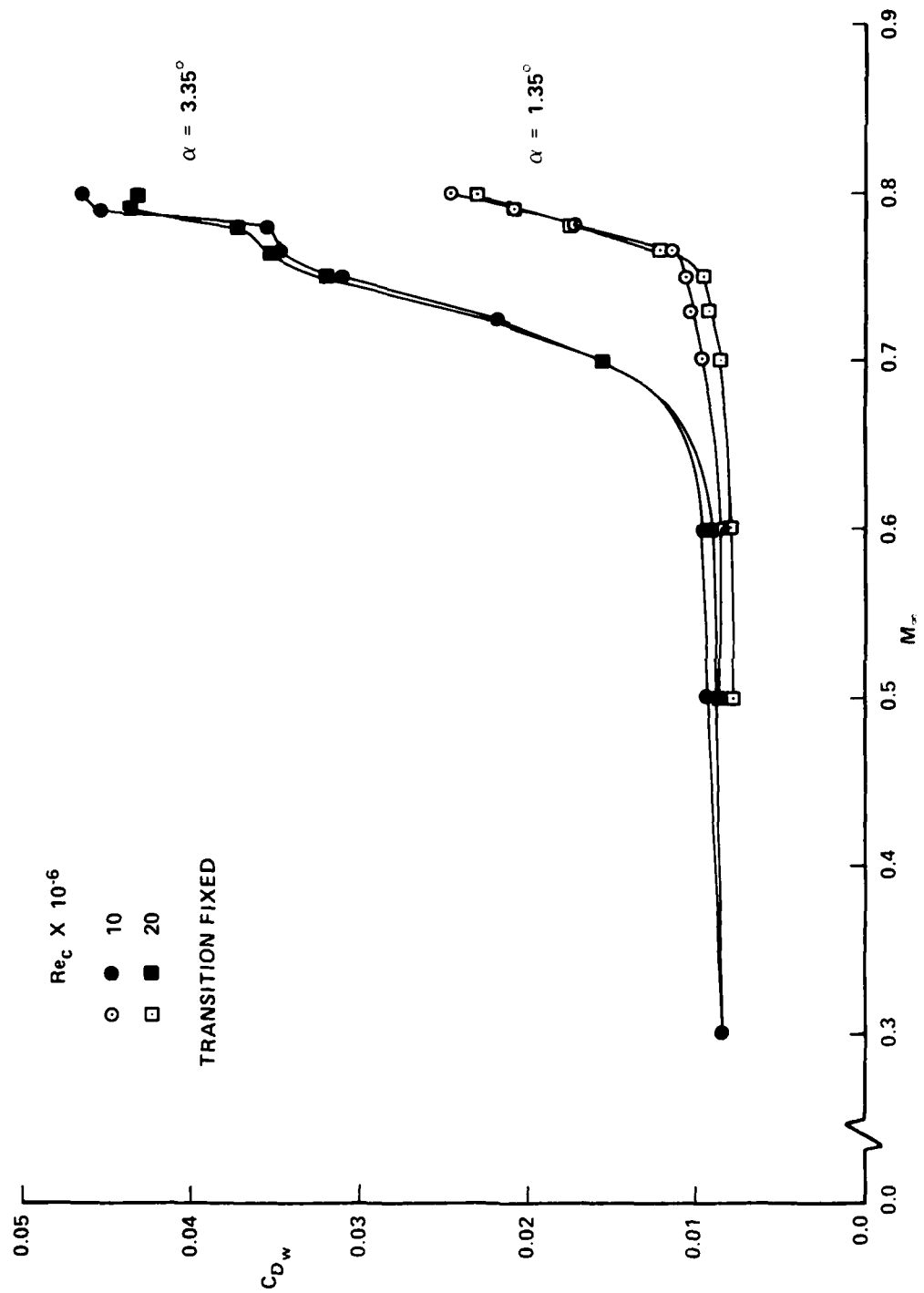

FIG. 17b: MACH NUMBER AND REYNOLDS NUMBER DEPENDENCE OF DRAG AT TWO ANGLES OF ATTACK WITH FIXED TRANSITION

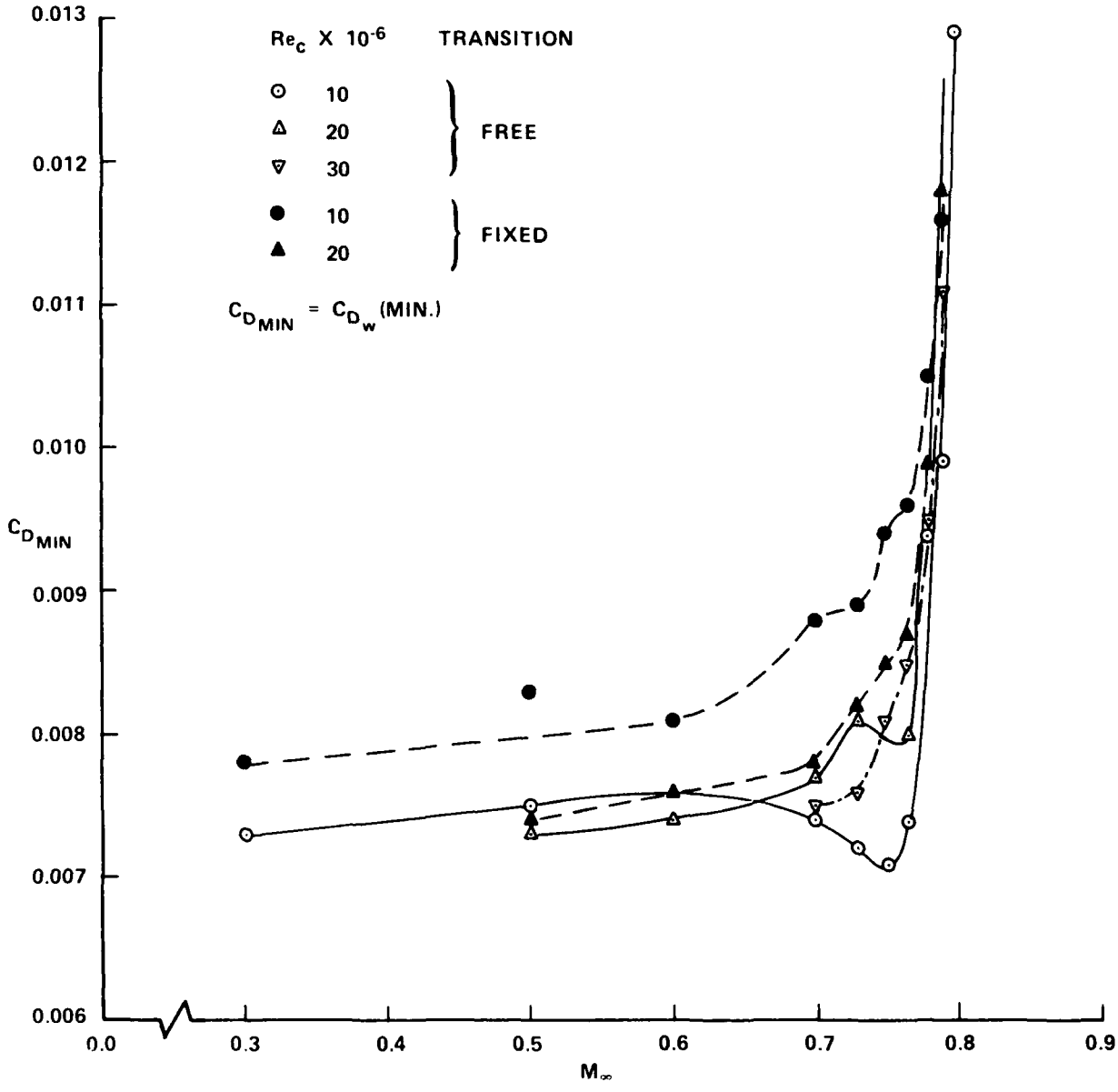

FIG. 18: MINIMUM DRAG VERSUS MACH NUMBER AT VARIOUS REYNOLDS NUMBERS WITH FIXED OR FREE TRANSITION

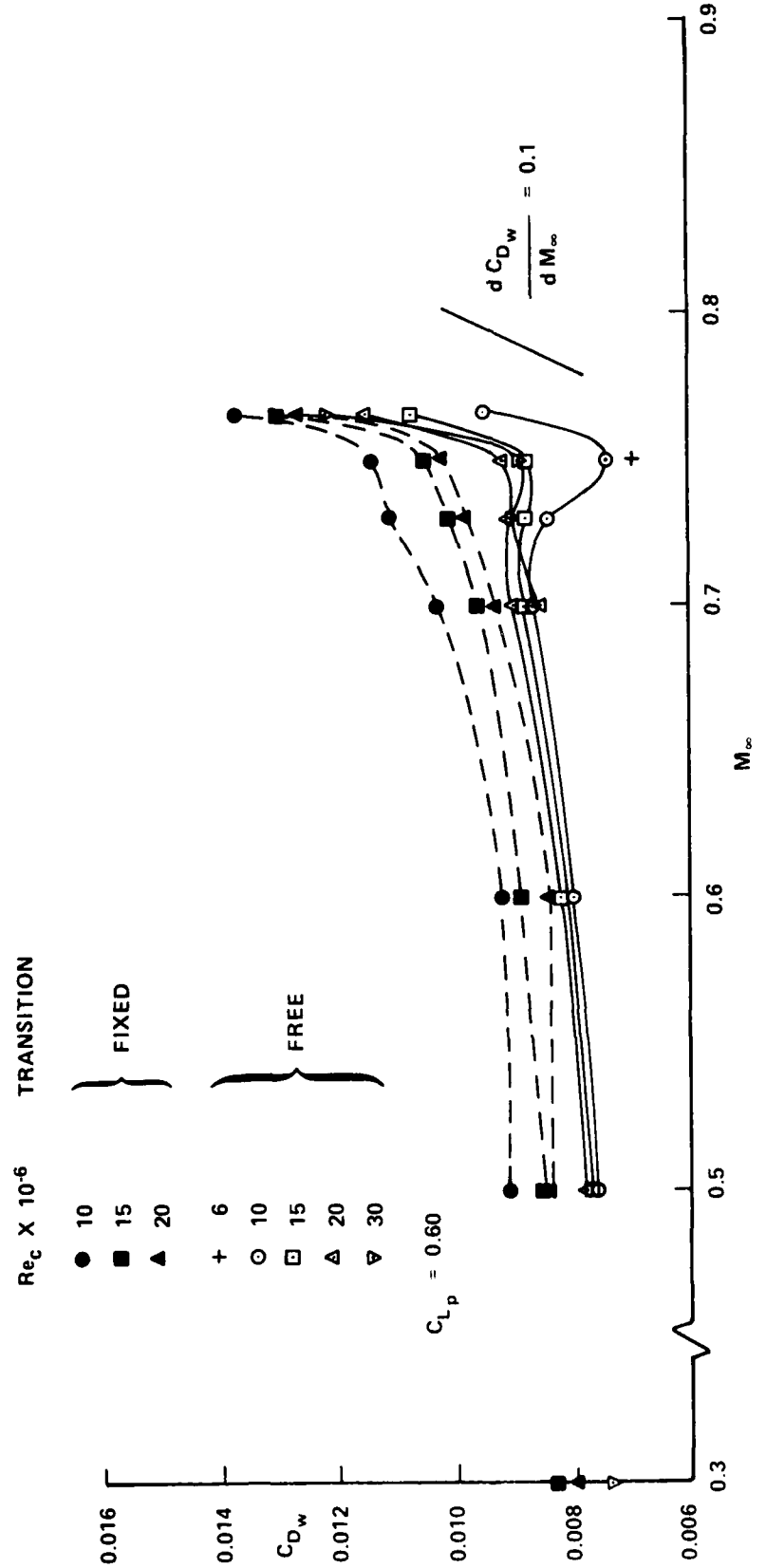

FIG. 19: DRAG AT C_{L_p} = 0.6 VERSUS MACH NUMBER AT VARIOUS REYNOLDS NUMBERS WITH FIXED OR FREE TRANSITION

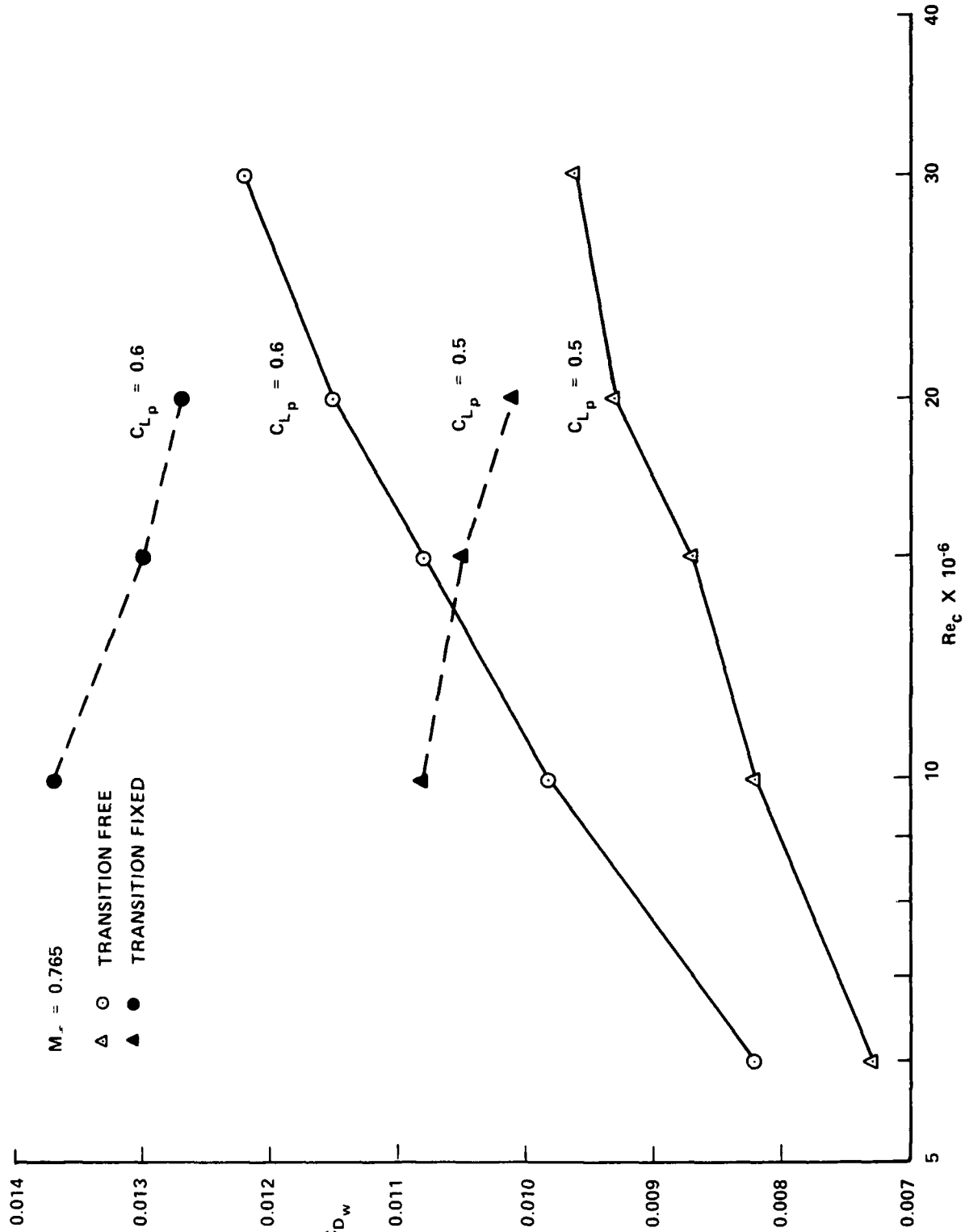

FIG. 20: REYNOLDS NUMBER DEPENDENCE OF DRAG AT M_∞ = 0.765, C_{L_p} = 0.5, 0.6 WITH FIXED OR FREE TRANSITION

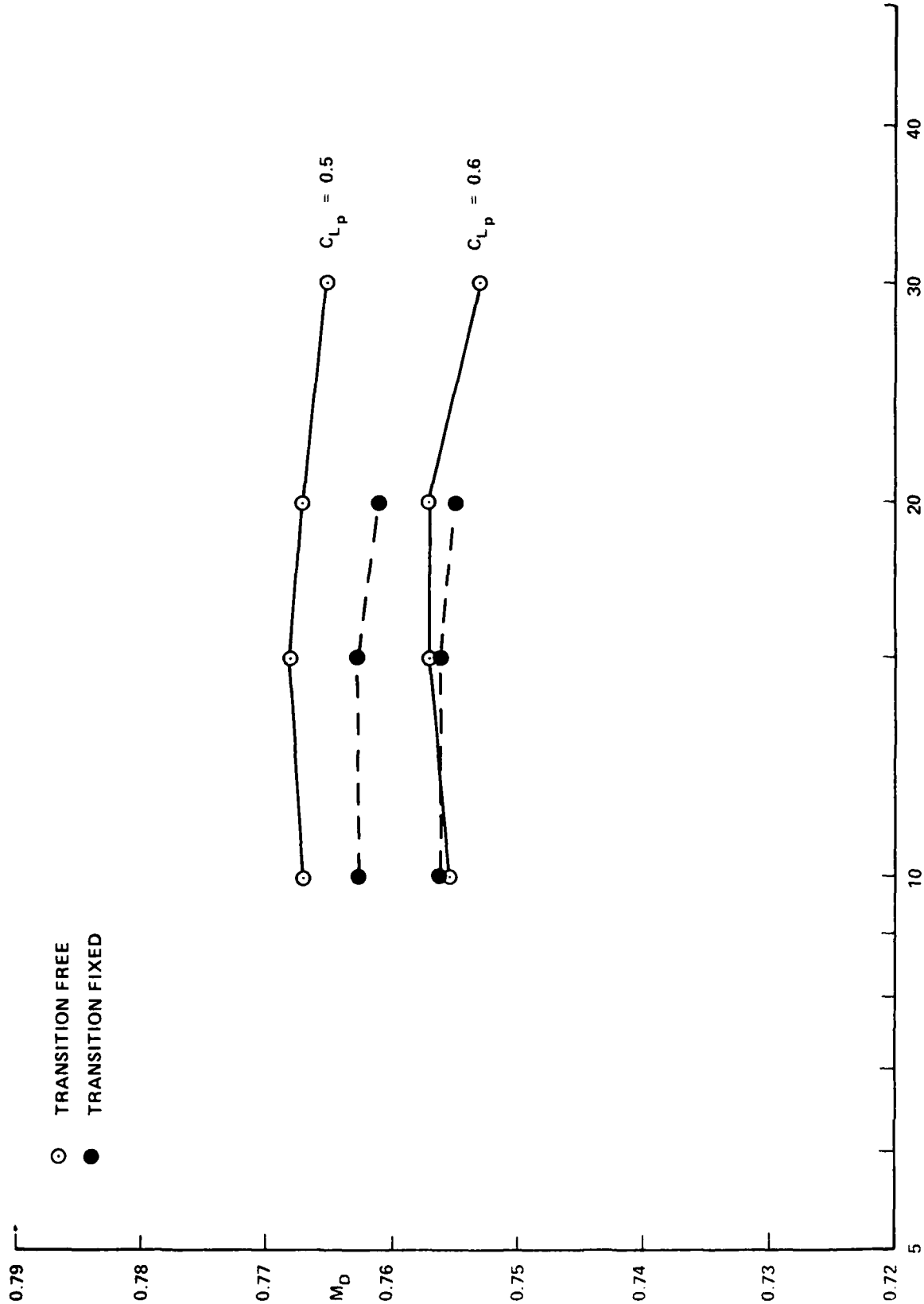

FIG. 21: REYNOLDS NUMBER DEPENDENCE OF DRAG WITH MACH NUMBER FOR TWO LIFT CONDITIONS WITH FIXED AND FREE TRANSITION

REPORT DOCUMENTATION PAGE / PAGE DE DOCUMENTATION DE RAPPORT

REPORT/RAPPORT	REPORT/RAPPORT
NAE-AN-49 (1a)	NRC No. 28595 (1b)
REPORT SECURITY CLASSIFICATION / CLASSIFICATION DE SÉCURITÉ DE RAPPORT	DISTRIBUTION (LIMITATIONS)
UNCLASSIFIED (2)	UNLIMITED (3)

TITLE/SUBTITLE/TITRE/SOUS-TITRE

Analysis of Experimental Data for CAST 10-2/DOA1 Supercritical Airfoil at High Reynolds Numbers (4)

AUTHOR(S)/AUTEUR(S)

Y.Y. Chan (5)

SERIES/SÉRIE

Aeronautical Note (6)

CORPORATE AUTHOR/PERFORMING AGENCY/AUTEUR D'ENTREPRISE/AGENCE D'EXÉCUTION

(7)

SPONSORING AGENCY/AGENCE DE SUBVENTION

National Research Council Canada
(8) National Aeronautical Establishment — High Speed Aerodynamics Laboratory

DATE	FILE/DOSSIER	LAB. ORDER / COMMANDE DU LAB.	PAGES	FIGS/DIAGRAMMES
Jan. 1988 (9)	(10)	(11)	68 (12a)	21 (12b)

NOTES

(13)

DESCRIPTORS (KEY WORDS)/MOTS-CLÉS

1. Supercritical wings,
2. Reynolds number,
3. Airfoils — Supercritical,

(14)

SUMMARY/SOMMAIRE

Experimental data obtained in the NAE Two-Dimensional Test Facility for CAST 10-2/DOA2 supercritical airfoil have been analyzed for the effects of Reynolds number, transition fixing and Mach number. The data were obtained for Reynolds numbers from 6 to 30 million and Mach numbers from 0.3 to 0.8 with fixed and free transitions. The analysis indicates that the aerodynamic parameters of the airfoil depend strongly on Reynolds number and transition fixing. Above Reynolds number 10 million the trends of dependency on Reynolds number with free or fixed transition can be established. For lower Reynolds number, the long stretch of laminar boundary layer over the airfoil alters the flow characteristics significantly and the data do not follow the trends for high Reynolds numbers.

(15)

END

DATE

FILMED

6-1988

DTIC